COMETARY ACTIVITY IN 2060 CHIRON

JANE X. LUU[a),b),c)]
Department of Earth, Atmospheric, and Planetary Sciences, Massachusetts Institute of Technology, Room 54-410, Cambridge, Massachusetts 02139

DAVID C. JEWITT[a),b),c)]
Institute for Astronomy, University of Hawaii, 2680 Woodlawn Drive, Honolulu, Hawaii 96822
Received 2 April 1990; revised 14 May 1990

ABSTRACT

We present the results of a 2 yr investigation of cometary activity in 2060 Chiron. The investigation is based on charge-coupled device (CCD) photometry and spectroscopy taken at the Mauna Kea, Kitt Peak, and MDM Observatories, with Chiron in the $11.2 \leqslant R \leqslant 12.6$ AU heliocentric distance range. The new photometry includes an image of 20 000 s effective integration, a new rotational light curve, the surface brightness profile of the coma at three epochs, and near-ultraviolet narrowband photometry taken to search for Rayleigh scattering from small particles in the coma. The spectroscopy from 1989 and 1990 was obtained to search for molecular emissions, and to study the shape of the reflected continuum of the nucleus and coma. Major results include the detection of impulsive brightening on a timescale of hours (to be distinguished from the slow rise in the total light observed in 1987–1990), evidence for a secular change in the blue portion of the reflectivity spectrum of the nucleus, no evidence for Rayleigh scattering in the near ultraviolet, and an upper limit to the column density of CO^+ ions in the coma. We also find that the surface brightness gradient of the coma of Chiron is steep and variable: it cannot be matched by steady-state models, compatible with our detection of transient mass loss at high rates. The photometric range of the rotational light curve is diminished in proportion to the local cross section of the coma, showing that the coma of Chiron is optically thin. We find that the mean mass loss rate needed to produce the observed coma is of order 1 kg s^{-1}, and that this rate can be supplied by sublimation of ices with the volatility of CO or CO_2 from a small fraction of the nucleus surface.

I. INTRODUCTION

Since its discovery in 1977 (Kowal 1977), 2060 Chiron has been regarded as an unusual asteroid with peculiar orbital characteristics: no other asteroid has been discovered at such a large distance (beyond the orbit of Saturn). The chaotic, cometlike, Saturn-crossing orbit of 2060 Chiron has provoked many questions about the physical nature of this body, including speculation on the possibility that Chiron is in fact a comet (e.g., Kresák 1979). The speculation was finally confirmed in 1988 by reports of sustained nonasteroidal brightening in Chiron (Tholen, Hartmann, and Cruikshank 1988), and the presence of a resolved coma was reported in 1989 (Meech and Belton 1989; Hartmann *et al.* 1990). A graphical summary of the photometric behavior of Chiron is given in Fig. 1, where we have plotted the photometry compiled by Hartmann *et al.* (1990), plus more recent observations of Chiron that are known to us (including those to be described in this paper). Figure 1 shows the absolute magnitude (i.e., the magnitude corrected for the inverse square law and for phase darkening) versus the date of observation. It is evident that the years 1980–1987 represent a "faint state," in which the absolute red magnitude is $\overline{H_R} = 6.3 \pm 0.1$, while Chiron is brighter in the interval 1988–present, by up to 1 mag. As we will discuss in Sec. III, the most recent observations show that $\overline{H_R}$ peaked in late 1988, and has since been in decline. The observations pre-1980 hint at an earlier period of outburst, but we are unsure of the accuracy of this "historical" photometry (see Bus *et al.* 1989 for a description).

The discovery of cometary activity in Chiron is not the final answer to a nagging question, but is the prelude to a great many problems to be resolved, particularly those concerning cometary activity at great distances. For instance, what is the cause of cometary activity in Chiron at heliocentric distance $R \sim 12$ AU? Does the faint state signify a complete lack of activity in Chiron, or is low level activity a persistent feature, as it is in the comet P/Schwassmann–Wachmann 1 at $R \sim 6$ AU (Jewitt 1990a)? Chiron is an order of magnitude larger than typical short-period comet nuclei studied to date (A'Hearn 1988), although it is larger than the nucleus of P/Schwassmann–Wachmann 1 by a factor of only 5. Does the implied larger mass affect the structure of the coma in a discernible way? The basic characteristics of cometary activity on Chiron are unknown. What is the size and nature of the particles in the coma? What is the mass loss rate? What is the physical process which controls the mass loss rate? Is the activity in Chiron typical of activity in all dynamically new comets as they approach the sun for the first time, or is it an artifact of the unusually large size of the nucleus? How is the activity related to activity seen in other distant comets, if at all?

In this paper, we present new charge-coupled device (CCD) photometric and spectroscopic observations of 2060

[a)] Visiting Astronomer at the Canada–France–Hawaii Telescope, operated by the National Research Council of Canada, the Centre National de la Recherche Scientifique de France, and the University of Hawaii.
[b)] Visiting Astronomer, Kitt Peak National Observatory, National Optical Astronomy Observatories, operated by the Association of Universities for Research in Astronomy Inc., under contract with the National Science Foundation.
[c)] Visiting Astronomer at the Michigan–Dartmouth–MIT (MDM) Observatory, Kitt Peak, which is operated by a three-university consortium consisting of University of Michigan, Dartmouth College, and MIT.

 0004-6256/90/030913-20$00.90

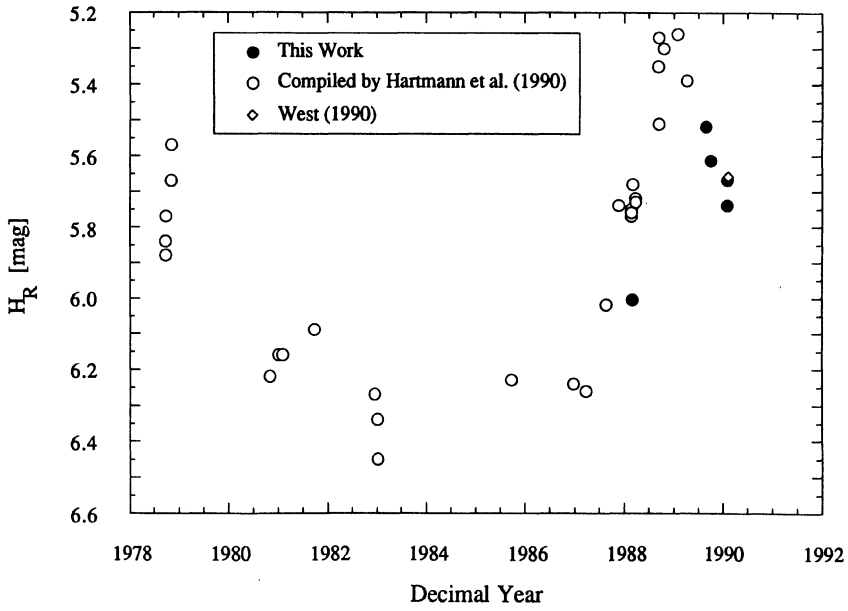

FIG. 1. Integrated photometry reduced to absolute magnitudes in the IAU Commission 20 (Bowell *et al.* 1989) system and plotted as a function of the date of observation. The data compiled from Hartmann *et al.* (1990) were transformed from H_V to H_R by $H_R = H_V - 0.37$. Errors are generally too small to be seen at the scale of the plot.

Chiron taken over a period of 2 yr (1988–1990). The photometric observations include a new rotational light curve of Chiron, a newly refined rotation period, recent developments of its long-term photometric behavior and surface brightness profiles, a deep image of the coma of Chiron (effective integration time $= 2\times10^4$ s), and narrowband images at wavelengths ranging from 3200 to 6840 Å. The spectroscopic data include moderate resolution CCD spectra (10–20 Å FWHM) in 1989 and 1990. We combine the new data with previous photometry by Bus *et al.* (1989) and Hartmann *et al.* (1990); the results of the observations and their constraints on the questions listed above are the subject of this paper.

In the following sections we describe the observational methods (Sec. II), the results of photometry (Sec. III), and spectroscopy (Sec. IV), and we suggest interpretations of the data in Sec V.

II. OBSERVATIONS

a) CCD Photometry

CCD photometry of 2060 Chiron was obtained at the Michigan–Dartmouth–MIT (MDM) 2.4 m telescope on Kitt Peak in February 1988, and at the University of Hawaii (UH) 2.24 m telescope on Mauna Kea in August and September 1989, and in January 1990. The modes of operation of the telescopes and their respective CCD detectors are as follows:

The MDM 2.4 m telescope was used at the Cassegrain $f/7.5$ focus. The guiding was controlled by the "MIS," which is a combination of finder and guider cameras developed by Matt Johns. The MIS, as well as the telescope pointing and most of the CCD functions, is in turn controlled by Sun computers which are operated by the observers. The detector used on the 2.4 m was the "MASCOT," a 390×584 TI4849 CCD with 22 μm pixels and a low readout noise (10 electrons per pixel). Enclosed in the MASCOT is a set of reimaging optics, allowing the reduction of the telescope focal ratio from $f/7.5$ to an effective focal ratio of $f/2.7$; the resulting image scale is 0.63 arcsec/pixel. The telescope was tracked at sidereal rate at all times.

At the UH 2.24 m telescope we used a GEC 385×576 CCD, located at the $f/10$ Cassegrain focus. In August 1989 and January 1990, the GEC was used without reimaging optics, resulting in an image scale of 0.20 arcsec per 22 μm pixel. In September 1989, the GEC was used in conjunction with a focal reducer, giving a reduced image scale of 0.86 arcsec/pixel. Like the TI4849, the GEC CCD is characterized by high linearity and a low readout noise (six electrons per pixel). The telescope was tracked at sidereal rate at all times and the integration times were selected so that the trailing was less than or comparable to the seeing disk during an exposure. Chiron was moving sufficiently slowly (<12 arcsec/hr) that the integration times were not severely limited by its motion. The configurations of the instruments used in the CCD photometry observations are summarized in Table I.

All CCD images were reduced and calibrated using standard methods. First, a bias (zero exposure) level was subtracted from each image. The pixel-to-pixel sensitivity variations were then removed by dividing by a bias-subtracted "flat field." Several different flat field construction schemes were tried, including dome flats and twilight sky flats. However, the optimum flattening was obtained by using the data frames themselves to determine the flat field shape. Stars and other objects in the data frames were removed from the flat field by computing the median of a large number of shifted sky images (typically 40). The reduced images were "flat," i.e., the sensitivity was uniform, to $\sim0.7\%$ across the full width of the chip, and to $\leqslant0.4\%$ on linear scales $\leqslant100$ pixels. A typical flattened CCD image of Chiron from 1990 January 29 is shown in Fig. 2 [Plate 87].

Flux calibration of the images was performed using standard stars from Landolt (1983). The images were corrected for nightly extinction by using photometry of field stars from the Chiron images and photometry of the Landolt stars taken at different airmasses. All observations were made under photometric conditions, with typically 1.5″ full width at half

TABLE I. Telescope configurations.

UT Date	Telescope	Instrument	Angular scale ("/pixel)	Work[a]
1988 February 29	MDM 2.4 m	MASCOT	0.63	BP
1989 February 4–8	KPNO 2.1 m	GoldCam	0.79	S
1989 August 25	UH 2.24 m	GEC	0.20	BP
1989 September 30	UH 2.24 m	GEC	0.86	BP
1990 January 29	UH 2.24 m	GEC	0.20	BP
1990 January 30	UH 2.24 m	GEC	0.20	BP, NP
1990 February 4–5	CFHT 3.6 m	Herzberg	0.57	S

[a] BP = broadband photometry, NP = narrowband photometry, and S = spectroscopy.

maximum (FWHM) seeing on Kitt Peak and 0.9" FWHM seeing on Mauna Kea. The absolute uncertainties in the Chiron photometry were ± 0.008 to ± 0.010 mag for the Mauna Kea data and ± 0.01 to ± 0.02 for the Kitt Peak data (the higher quality of the Mauna Kea photometry is largely a result of the superior seeing at that site). All broadband observations (which comprise most of the photometry) were obtained in the Mould R filter ($\lambda_{central} = 6500$ Å) to exploit the maximum quantum efficiency of the CCDs and to minimize atmospheric extinction. In addition, narrowband images were taken at the UH 2.24 m telescope, using filters selected from the International Halley Watch (IHW) narrowband filter set. The specifications of these filters can be found in Table VII of this work. The narrowband images were flux calibrated using standard stars from Massey *et al.* (1988).

Our coverage of Chiron spans a 2 yr period (1988–1990), during which the heliocentric distance of Chiron decreased from 12.60 to 11.25 AU. The geometric circumstances of the observations are listed in Table II.

b) CCD Spectroscopy

CCD spectra of Chiron were obtained at the Kitt Peak National Observatory (KPNO) 2.1 m in February 1989 and at the Canada–France–Hawaii 3.6 m telescope (CFHT) on Mauna Kea in February 1990. At the KPNO 2.1 m we used the GoldCam spectrograph, mounted at the $f/7.7$ Cassegrain focus. The GoldCam contained an 800×800 TI CCD with a readout noise of nine electrons per pixel. Using a 150 lines/mm grating (blazed at $\lambda = 5000$ Å) in the first order, we obtained a dispersion of 4.9 Å/pixel, and a spatial resolution of 0.79"/pixel. The slit was oriented north–south, with projected dimensions $2.8" \times 150"$. With this configuration, the resulting spectra had a spectral coverage of $3600 \leqslant \lambda \leqslant 7400$ Å, and an effective resolution of ~ 20 Å FWHM.

TABLE II. Viewing parameters.

UT Date	R (AU)	Δ (AU)	α (°)	Scale (km/")
1988 February 29	12.60	12.33	4.4	8966
1989 February 4	11.95	11.22	3.3	8159
1989 February 8	11.94	11.26	3.5	8188
1989 August 25	11.56	12.20	3.8	8872
1989 September 30	11.49	11.60	4.9	8436
1990 January 29	11.26	10.38	2.4	7548
1990 January 30	11.26	10.39	2.4	7556
1990 February 4	11.25	10.42	2.8	7577
1990 February 5	11.25	10.43	2.9	7585

We used the Herzberg spectrograph at the CFHT 3.6 m on UT 1990 February 4–5. The detector inside the Herzberg was the "PXH1," a 512×512 RCA CCD with 20 μm pixels and a very low readout noise of 2.7 electrons. The optics in the Herzberg have been coated for optimal UV transmission. All Herzberg spectra presented in this paper were taken with a 300 lines/mm grating blazed at $\lambda = 4200$ Å and used in first order. This configuration yielded a dispersion of 3.3 Å/pixel and a spatial resolution of 0.57"/pixel. The grating position was changed between the two nights, in order to maximize the wavelength coverage: the coverage was 4460–6150 Å on 1990 February 4, and 3650–5340 Å on 1990 February 5. The $1.5" \times 130"$ slit was oriented north–south and the final effective spectral resolution was 10 Å FWHM. A summary of the details of the CCD configurations is provided in Table III.

At both telescopes, Chiron was located using the acquisition finder TV and was guided manually by monitoring a down-looking guider TV. We estimated the maximum guiding errors to be $\leqslant 0.5$ arcsec, small compared to the slit width. At least two independent spectra of Chiron were taken on a given night as a check on the repeatability of the spectra; the individual spectra from each night were subsequently combined to produce a single spectrum with improved signal to noise. Both spectrographs yielded high-quality spectra, the evidence of which is the repeatability of the signals measured on different nights. Further evidence of the quality of the Kitt Peak data can be found in Luu and Jewitt (1990), since the 1989 Chiron spectra were taken in conjunction with the program described in that paper.

Spectra of helium-neon-argon lamps (at the KPNO 2.1 m) and of iron-argon lamps (at the CFHT) were taken frequently throughout each night for wavelength calibration. Flux calibration of the spectra was performed using standard stars from Stone (1977). The standard star observations were scheduled to coincide closely in airmass and in time with the Chiron observations, so as to minimize extinction and temporal variability problems. The standard star-Chiron airmass difference was $\leqslant 0.05$ for all spectra presented. We also observed solar analogs in anticipation of computing the reflectivity gradients (colors) of the spectra. The solar analogs observed at both telescopes were Hyades 64 and 106 (Hardorp 1978, 1980). A large number (~ 50) of flat fields (spectra of a continuum source) and bias frames were taken at the beginning of each night for later data reduction.

Most of the spectral data reduction was accomplished using the software package IRAF. The Chiron spectra were reduced according to standard procedures described in Luu and Jewitt (1990), except in the sky subtraction procedure. The sky background was subtracted from the Chiron spectra

TABLE III. CCD spectroscopy log.

Telescope	f/ratio	Instrument	CCD size	Read noise	$\Delta\lambda$ FWHM	λ range	Spatial scale	Slit size	Dispersion
UT 1989 February 4 and 8									
2.1 m	7.7	GoldCam	800×800	9 e^-	20 Å	3600–7200 Å	0.79″/pixel	2.8″×150″	4.9 Å/pixel
UT 1990 February 4									
3.6 m	8.0	Herzberg	516×516	2.7 e^-	10 Å	4460–6150 Å	0.57″/pixel	1.5″×131″	3.3 Å/pixel
3.6 m	8.0	Herzberg	516×516	2.7 e^-	10 Å	3650–5340 Å	0.57″/pixel	1.5″×131″	3.3 Å/pixel

using two different methods: (1) the sky background was extracted directly from the Chiron spectrum by spatial interpolation (the standard method). The resulting reduced spectrum is used to compute the continuum spectrum of the object; (2) the sky background was extracted from a near-simultaneous sky frame taken 600″ away from Chiron. The reason for this procedure was to avoid self-subtracting any gaseous coma generated by Chiron itself; the resulting spectrum was used to search for gaseous emissions in Chiron.

III. PHOTOMETRY

In Table IV, we present a summary of the photometry, including the values of mean R magnitude, $\overline{m_R}$, the corresponding absolute magnitude $\overline{H_R}$ (as defined in the Appendix of Bowell *et al.* 1989), and the light curve range Δm_R obtained over the 2 yr period. The new integrated photometry (Fig. 1) shows that Chiron reached a peak absolute magnitude $\overline{H_R} \sim 5.25$ in 1988–1989, and that the brightness has decreased by about 0.5 mag in the 1.1 yr since maximum. The rate of decline of the absolute magnitude is ~0.05 millimag/hr, compared to the rate of change in the 1988–1989 period of ~0.1 millimag/hr. Detailed descriptions of the individual observations follow in the next four subsections.

a) February 1988 (R = 12.60 AU)

The Chiron aperture photometry is presented in Table V and plotted as a function of time in Fig. 3. The figure shows nonrandom variations in the magnitude having a range of order $\Delta m_R = 0.09$ mag, centered on $\overline{m_R} = 17.11 \pm 0.01$. The time coverage is too sparse to extract a rotation period, but the sampled light curve appears consistent with the published rotation period (5.92 hr) and light curve range (0.09 mag; Bus *et al.* 1989) in the preactive phase. Using the slope parameter $G_R = 0.70$ (Bus *et al.* 1989), we derive the absolute magnitude

$$\overline{H_R} = 6.01 \pm 0.01 \text{ mag.} \quad (1)$$

This is ~0.3 mag brighter than the mean absolute in the supposed "faint state" period 1980–1986 ($\overline{H_R} = 6.3 \pm 0.1$), and compatible with activity in 2060 Chiron. For comparison, we note that a 0.45 mag increase in brightness was reported in March 1988 (Buss, Bowell, and French 1988).

Chiron appears stellar in all 12 images from this month. We shifted the images to remove the motion of Chiron with respect to the fixed stars, then computed the median of the shifted images to search for a possible faint coma. We also computed the median of the original unshifted images to obtain a profile of a field star for comparison. Figure 4 is a plot of the surface brightness profiles of Chiron and of a field star, computed from the median image (effective integration time = 6095 s). The surface brightness profile $B(r)$, where r is the distance from the nucleus, is computed from the mean intensity measured in a set of concentric annuli of 0.5″ in width. The accuracy of the profile is limited only by the accuracy of subtraction of the background sky. We estimate that the errors in the sky subtraction are $\leqslant \pm 0.5\%$, and the plotted error bars indicate the effect of a 0.5% error in the level of the sky on the surface brightness profiles. The figure shows that there is no evidence for a resolved coma at this epoch. A summary of surface photometry results can be found in Table VI.

TABLE IV. Photometry parameters.

UT	$\overline{m_R}$ (mag)	$\overline{H_R}$ (mag)	Δm_R (mag)
1998 February 29	17.11 ± 0.01	6.01 ± 0.01	0.09
1989 August 25	16.40 ± 0.01	5.52 ± 0.01	—
1989 September 30	16.40 ± 0.01	5.61 ± 0.01	⩾0.05
1990 January 29	16.18 ± 0.01	5.74 ± 0.01	0.045
1990 January 30	16.11 ± 0.01	5.67 ± 0.01	—

b) August 1989 (R = 11.56 AU)

Two observations of Chiron were obtained under photometric conditions on UT 1989 August 25 (Tables IV and V). At this time, Chiron had the mean apparent magnitude $\overline{m_R} = 16.40 \pm 0.01$, corresponding to the absolute magnitude

$$\overline{H_R} = 5.52 \pm 0.01, \quad (2)$$

or a 0.5 mag brightening since February 1988 and 0.72 mag brighter than in 1980–1986. Bright sky resulting from moonlight prevents the computation of a useful surface brightness profile in these data.

c) September 1989 (R = 11.49 AU)

Seven photometric observations were obtained on UT 1989 September 30 (Tables IV and V). The mean apparent magnitude was $\overline{m_R} = 16.40 \pm 0.01$ mag, corresponding to

$$\overline{H_R} = 5.61 \pm 0.01 \text{ mag.} \quad (3)$$

A relatively large image scale (0.86″/pixel) and a bright star in the field hinders the visibility of a coma in a single image. To search for evidence of a coma, we shifted the seven images and computed the median, producing a final image with an effective integration time of 780 s. Similarly, a median from the original unshifted images was computed to pro-

TABLE V. Broadband photometry of 2060 Chiron.

UT Date	UT hr[a]	$m_R \pm \sigma_{m_R}$ (mag)	H_R (mag)
1988 February 29	2.6861	17.10 ± 0.02	6.00 ± 0.02
1998 February 29	2.7797	17.08 ± 0.02	5.98 ± 0.02
1988 February 29	2.9175	17.07 ± 0.02	5.96 ± 0.02
1988 February 29	3.0389	17.09 ± 0.02	5.99 ± 0.02
1988 February 29	3.1678	17.11 ± 0.02	6.01 ± 0.02
1988 February 29	3.2875	17.10 ± 0.02	6.00 ± 0.02
1988 February 29	3.4086	17.12 ± 0.02	6.02 ± 0.02
1988 February 29	3.5292	17.12 ± 0.02	6.02 ± 0.02
1988 February 29	3.6517	17.14 ± 0.02	6.04 ± 0.02
1988 February 29	3.7728	17.15 ± 0.02	6.05 ± 0.02
1988 February 29	5.5294	17.11 ± 0.02	6.00 ± 0.02
1988 February 29	5.6536	17.10 ± 0.02	5.99 ± 0.02
1989 August 25	14.3342	16.38 ± 0.01	5.50 ± 0.01
1989 August 25	14.4764	16.41 ± 0.01	5.53 ± 0.01
1989 September 30	14.8669	16.37 ± 0.01	5.59 ± 0.01
1989 September 30	14.9792	16.39 ± 0.01	5.61 ± 0.01
1989 September 30	15.0250	16.40 ± 0.01	5.62 ± 0.01
1989 September 30	15.0694	16.42 ± 0.01	5.63 ± 0.01
1989 September 30	15.1178	16.39 ± 0.01	5.61 ± 0.01
1989 September 30	15.1667	16.40 ± 0.01	5.62 ± 0.01
1989 September 30	15.2147	16.41 ± 0.01	5.62 ± 0.01
1990 January 29	6.2367	16.231 ± 0.008	5.793 ± 0.008
1990 January 29	6.4022	16.217 ± 0.008	5.779 ± 0.008
1990 January 29	6.5669	16.197 ± 0.008	5.759 ± 0.008
1990 January 29	6.7261	16.192 ± 0.008	5.754 ± 0.008
1990 January 29	6.8880	16.198 ± 0.008	5.760 ± 0.008
1990 January 29	7.0494	16.192 ± 0.008	5.754 ± 0.008
1990 January 29	7.2083	16.197 ± 0.008	5.759 ± 0.008
1990 January 29	7.3806	16.203 ± 0.008	5.765 ± 0.008
1990 January 29	7.5436	16.195 ± 0.008	5.757 ± 0.008
1990 January 29	7.7119	16.205 ± 0.008	5.767 ± 0.008
1990 January 29	7.8931	16.203 ± 0.008	5.765 ± 0.008
1990 January 29	8.0594	16.212 ± 0.008	5.774 ± 0.008
1990 January 29	8.3840	16.201 ± 0.008	5.787 ± 0.008
1990 January 29	8.5533	16.225 ± 0.008	5.786 ± 0.008
1990 January 29	8.7300	16.224 ± 0.008	5.753 ± 0.008
1990 January 29	8.8770	16.191 ± 0.008	5.745 ± 0.008
1990 January 29	9.0380	16.183 ± 0.008	5.745 ± 0.008
1990 January 29	9.2014	16.183 ± 0.008	5.734 ± 0.008
1990 January 29	9.3653	16.172 ± 0.008	5.715 ± 0.008
1990 January 29	9.5194	16.153 ± 0.008	5.711 ± 0.008
1990 January 29	9.6794	16.149 ± 0.008	5.708 ± 0.008
1990 January 29	9.8390	16.146 ± 0.008	5.719 ± 0.008
1990 January 29	9.9940	16.157 ± 0.008	5.716 ± 0.008
1990 January 29	10.1510	16.154 ± 0.008	5.719 ± 0.008
1990 January 29	10.3069	16.157 ± 0.008	5.713 ± 0.008
1990 January 29	10.4860	16.151 ± 0.008	5.690 ± 0.008
1990 January 29	10.8010	16.140 ± 0.008	5.702 ± 0.008
1990 January 29	10.9567	16.167 ± 0.008	5.729 ± 0.008
1990 January 29	11.1120	16.177 ± 0.008	5.739 ± 0.008
1990 January 29	11.2660	16.172 ± 0.008	5.734 ± 0.008
1990 January 29	11.4340	16.173 ± 0.008	5.735 ± 0.008
1990 January 29	11.5944	16.174 ± 0.008	5.736 ± 0.008
1990 January 29	11.7503	16.161 ± 0.008	5.723 ± 0.008
1990 January 29	11.9031	16.154 ± 0.008	5.716 ± 0.008
1990 January 29	12.0570	16.157 ± 0.008	5.719 ± 0.008
1990 January 29	12.2131	16.176 ± 0.008	5.738 ± 0.008
1990 January 29	12.3790	16.154 ± 0.008	5.716 ± 0.008
1990 January 29	12.5322	16.132 ± 0.008	5.694 ± 0.008
1990 January 29	12.6894	16.134 ± 0.008	5.696 ± 0.008
1990 January 29	12.8460	16.128 ± 0.008	5.690 ± 0.008
1990 January 29	13.0164	16.143 ± 0.008	5.705 ± 0.008
1990 January 29	13.1730	16.137 ± 0.008	5.699 ± 0.008
1990 January 29	13.3453	16.121 ± 0.008	5.683 ± 0.008
1990 January 30	6.4917	16.12 ± 0.01	5.68 ± 0.01
1990 January 30	6.6208	16.10 ± 0.01	5.66 ± 0.01
1990 January 30	6.7369	16.13 ± 0.01	5.69 ± 0.01

[a] UT start of the integration.

duce a high signal-to-noise image of the background star field. From the median images, we calculate the surface brightness profiles of Chiron and a field star (plotted in Fig. 5). The profile of Chiron is unambiguously broader than that of the field star, and the coma is clearly visible as far as $r = 10''$ from the nucleus [$B(10'') = 25.3$ mag/arcsec^2]. It is possible that the visible coma extends further than 10", but the presence of a nearby star obliterates the profile at greater distances. We attempt to fit the surface brightness profile with a power law in which the slope index of the coma s is defined by

$$s = d \ln B(r)/d \ln r. \quad (4)$$

In the range $r = 6''$–$10''$, the best-fit index is

$$s = -1.5 \pm 0.1. \quad (5)$$

This is steeper than the case of a steady state, spherically symmetric coma ($s = -1$), but is consistent with the slope for a radiation pressure-affected coma ($s = -1.5$) (Jewitt 1990b). We are confident that the measured slope is the *intrinsic* (as opposed to the apparent) slope of the coma, since the fitted region is well away from the seeing disk ($\sim 1''$ FWHM). Indeed, our confidence is founded on experiments in which model comae were convolved with the actual seeing profile to test the effect of seeing on the outer coma gradient (see Sec. V*b* for more on convolved model comae). A summary of surface photometry results can be found in Table VI.

d) January 1990 (R = 11.26 AU)

Our most extensive coverage of Chiron was obtained on 1990 January 29–30 (Tables IV and V). All observations were taken under photometric conditions, with subarcsec seeing ($\sim 0.8''$) on UT January 29. A faint coma was clearly visible in all images, extending predominantly in the south–east direction, at position angle 157 ± 3° (1σ uncertainty). The uncertainty stems from the fact that the coma is diffuse and not well collimated (Fig. 2). The position angle of the coma is consistent with the projected antisolar direction on this date, which was at position angle 160°.

We plot the photometry from UT 1990 January 29 in Fig. 6(a). The figure shows systematic variations in integrated magnitude, and the variations are consistent with a 6 hr rotation period. Although the periodicity is reminiscent of the 1986 observations by Bus *et al.* (1989), the present light curve differs from previous photometry in two important respects:

(1) Superimposed on the periodic light curve is a steady brightening trend of $dm_R/dt \sim 15$ millimag/hr. This trend cannot be attributed to errors in the correction for atmospheric extinction since (a) the observations were made under photometric conditions, (b) the brightening is not correlated with the airmass, and furthermore, (c) field stars recorded in the same images as Chiron show no similar trend. The brightening trend in the light curve proves that, in addition to the already reported long-term (months to years) brightness variations, Chiron also exhibits short-term brightness variations (on timescales of hours). This provides direct evidence that (a) activity in Chiron is impulsive, and (b) that Chiron is active in 1990 January, even though the total magnitude is then in general decline (Fig. 1). The slope complicates the determination of a mean magnitude and range for the light curve; however, we adopt $\overline{m_R} = 16.18 \pm 0.01$ mag, corresponding to

$$\overline{H_R} = 5.74 \pm 0.01 \text{ mag}. \quad (6)$$

(2) After subtracting the brightening trend from the data [Fig. 6(b)], the range of the light curve is $\Delta m_R = 0.045$ mag, i.e., the photometric range of Chiron has decreased

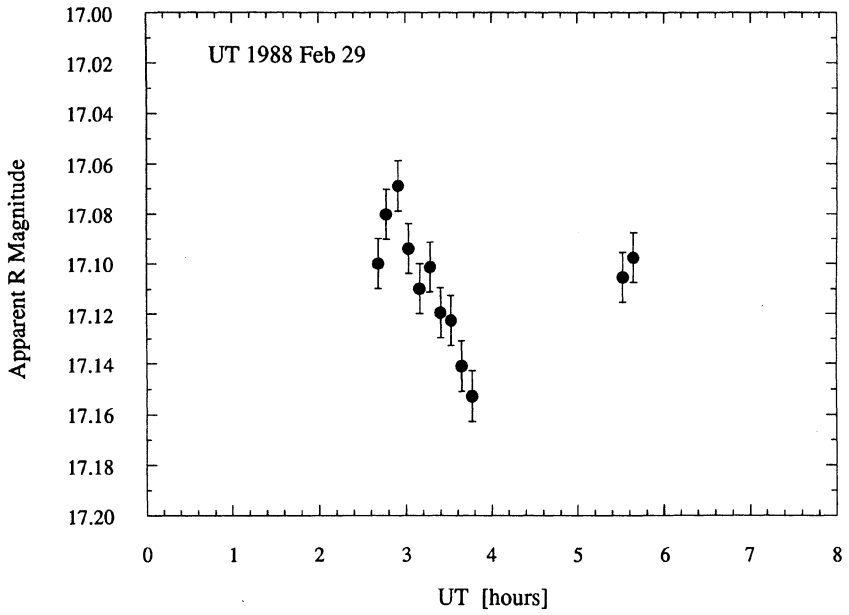

FIG. 3. Rotational light curve of 2060 Chiron obtained UT 1988 February 29 at the 2.4 m telescope of MDM Observatory. The range of variation is approximately 0.09 mag. Error bars are $1\sigma = 0.01$ mag.

from $\Delta m_{\rm Bus} = 0.088$ mag to $\Delta m_R = 0.045$ mag in ~ 3 yr. We show below that the decrease of the light curve range is compatible with dilution of light from the nucleus by an optically thin coma.

The photometry from UT 1990 January 29 and 30 is plotted in Fig. 7. The figure shows that the brightening trend of UT 1990 January 29 continued into UT January 30, although at a reduced rate. We conclude that, on UT 1990 January 30, Chiron had the mean "R" magnitude $\overline{m_R} = 16.11 \pm 0.01$ mag and the absolute magnitude

$$\overline{H_R} = 5.67 \pm 0.01 \text{ mag.} \quad (7)$$

We note that West (1990) reported $H_R = 5.66$ mag from independent observations on UT 1990 February 21. However, given the short-term variability of Chiron, the consistency between our photometry and that of West is probably coincidental.

We also obtained narrowband photometry of Chiron on UT 1990 January 30 with filters centered at 3200, 3650, 3871, 4060, 4260, 5139, and 6840 Å. The calibrated integrated magnitudes (within a 2.4″ radius aperture) are listed in Table VII. To compare the colors of Chiron with solar colors, the integrated magnitudes were converted into flux densities then divided by the tabulated solar flux densities of

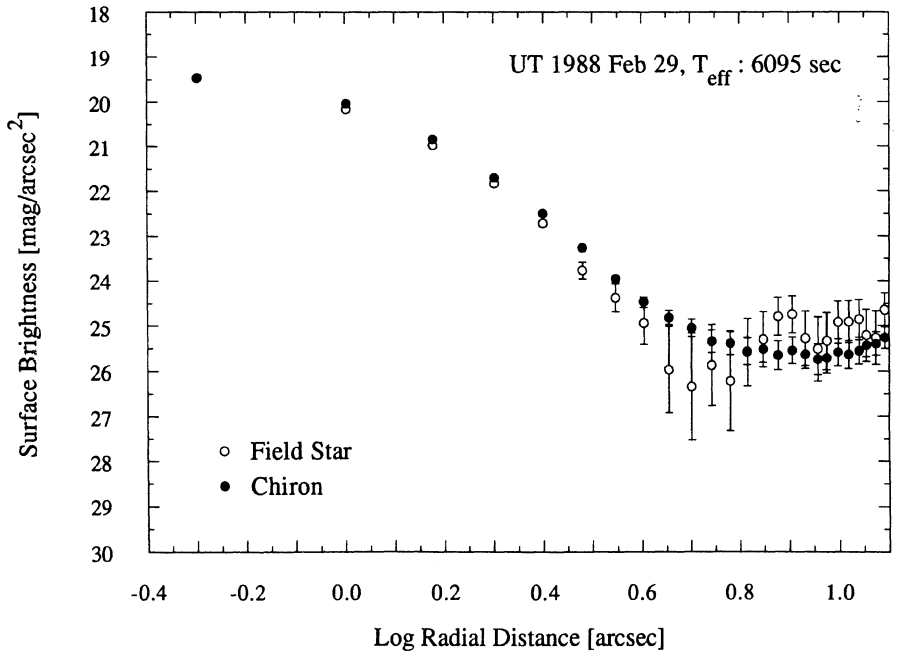

FIG. 4. Annular surface brightness profile obtained from stacked CCD images recorded UT 1988 February 29. The surface brightness (in R mag per arcsec^2) is plotted against the annulus radius, for Chiron and for a field star. Error bars on the surface-brightness profiles reflect uncertainties which would result from a $\pm 0.5\%$ error in the determination of the surface brightness of the surrounding night sky.

TABLE VI. Surface photometry of 2060 Chiron.

UT Date	r (arcsec)	$B(r)$ (mag/arcsec^2)
1988 February 29	6.5[a]	$\leqslant$25.57
1989 September 30	6.5	24.96 $\pm$ 0.09
1989 September 30	10.0[a]	25.22 $\pm$ 0.11
1990 January 29	6.5	25.38 $\pm$ 0.09
1990 January 29	12.5[a]	26.36 $\pm$ 0.12

[a] The largest radial distance at which we could measure the surface brightness with confidence. The coma may extend much further than this distance, but no reliable measurement was obtainable (either due to the very low surface brightness or contamination by a nearby star).

Arvesen, Griffin, and Pearson (1969). The conversion from magnitudes to flux densities was made according to the equation

$$F_\nu = 10^{-0.4(m+48.59)}, \quad (8)$$

(Massey *et al.* 1988), where F_ν (ergs s^{-1} cm^{-2} Å^{-1}) is the flux density and m is the narrowband magnitude as listed in Table VII. The Arvesen *et al.* solar fluxes were tabulated at much higher resolution than our data, hence we averaged the solar flux over the bandpass of each filter to arrive at a resolution comparable to ours. The reflectivities of Chiron are plotted as a function of wavelength in Fig. 8, where they are arbitrarily normalized to unity at 5139 Å. On this plot, a perfectly neutral reflector would appear as a horizontal line. The figure shows that Chiron is a very nearly neutral reflector at wavelengths $\lambda \geqslant 4600$ Å, but that the reflectivity decreases by $\sim$20% at wavelengths $3500 \leqslant \lambda \leqslant 4600$ Å, possibly indicative of an absorption feature. The $\lambda \geqslant 4600$ Å data are in agreement with the photometry of Hartmann *et al.* (1990) but we know of no previous short-wavelength data with which to compare Fig. 8. The shape of the narrowband reflectivity spectrum will be discussed later in connection with CCD spectra.

The coma is visible in the individual broadband images taken during January 1990 (see Fig. 2); however, the low surface brightness conceals a clear picture of its morphology. This was remedied by shifting and adding 40 of the 43 images taken on this night (the last three images were ignored due to deterioration in the seeing). The resulting image, shown in Fig. 9 [Plate 88], has an effective integration time of 20 000 s; it is of very high signal-to-noise ratio and is characterized by $\sim$0.8″ FWHM seeing. Field stars appear in this image in rows due to the canceled motion of Chiron. The coma is amorphous and elliptical in shape, with the long axis extending along the south–east and north–west directions. The figure shows that the visible coma extends at least as far as 8″ in the south–east direction (position angle $\sim 157 \pm 3°$) and in the north–west direction (position angle $\sim 337 \pm 3°$).

As may be seen in Fig. 9, a number of stars crossed the outer coma of Chiron during the 20 000 s integration. For this reason, the 20 000 s image is unsuitable for studies of the coma surface brightness profile. We selected nine images in which Chiron is relatively far from encroaching stars, and computed the median to produce a single star-free image of 4500 s effective integration. The nine images were shifted twice in order to produce two median images, one of Chiron and one of a field star (for comparison). The resulting surface brightness profiles of Chiron and the star are plotted in Fig. 10. The Chiron profile extends at least 13″ from the nucleus, whereas the stellar profile starts a steep decline in surface brightness at 3″. A comparison of the stellar profiles of September 1989 (Fig. 5) and January 1990 (Fig. 10) shows that the two are considerably different from one another, with the stellar image of January 1990 being much more concentrated. We attribute the change in image quality to better seeing and to the realuminizing of the UH 2.2 m mirror in October 1989, resulting in improved wings in the

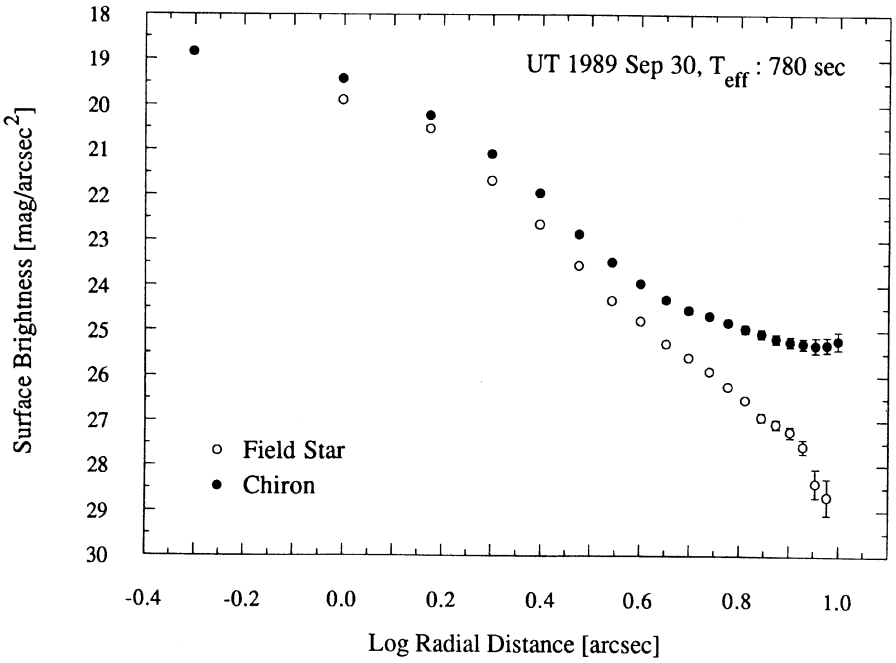

FIG. 5. Same as Fig. 4, but for data taken on UT 1989 September 30, at the UH 2.2 m. Plotted error bars show the effect of a $\pm$0.3% error in the surface brightness of the night sky.

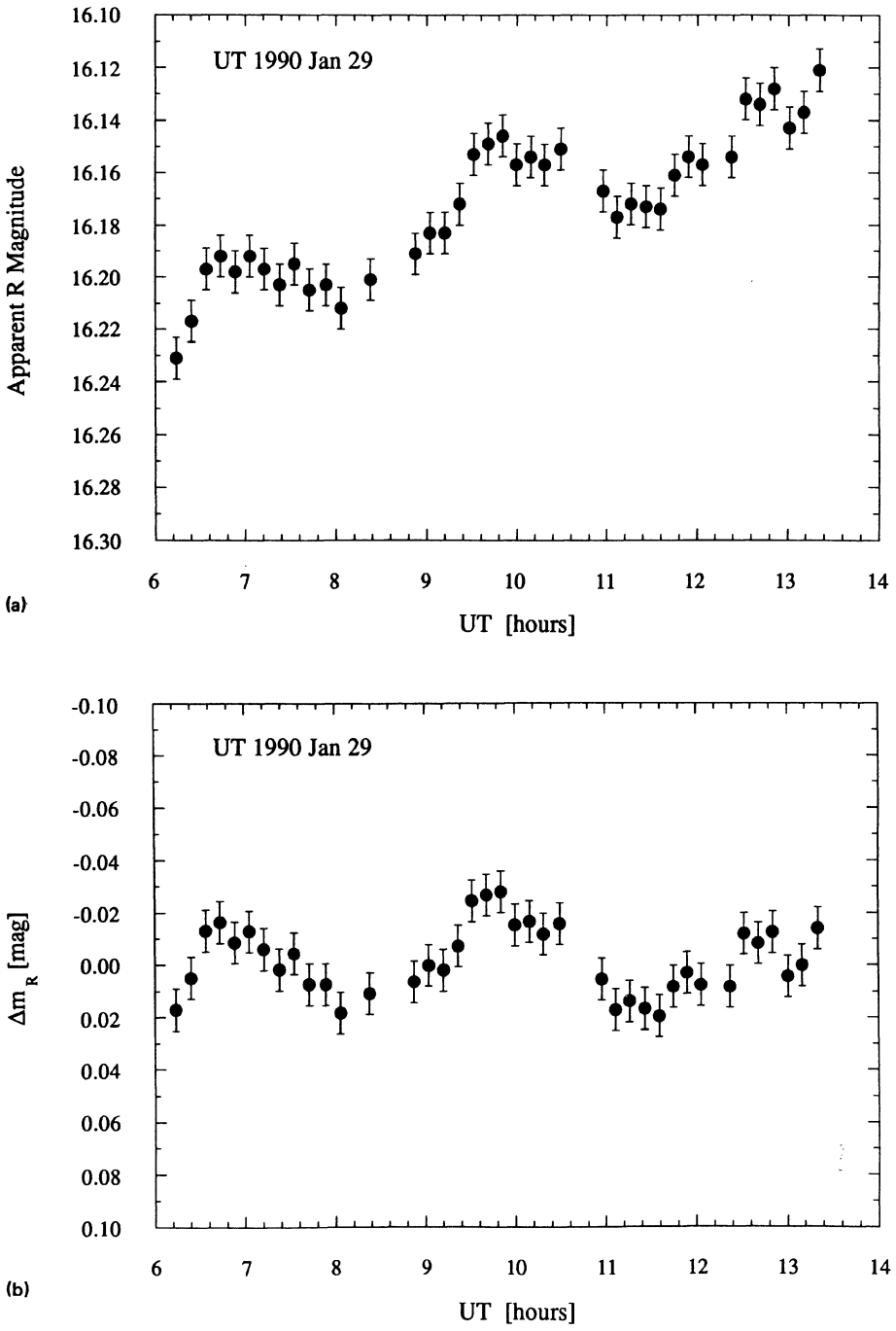

FIG. 6. (a) Rotational light curve of 2060 Chiron obtained UT 1990 January 29 at the UH 2.2 m telescope on Mauna Kea. The rotational variations appear superposed on a linear brightening trend. Error bars are $1\sigma = 0.008$ mag. (b) Same data as in (a) but with the linear trend removed.

stellar image. Fitting the surface brightness profile of Chiron in Fig. 10 with a power law in the 6″–10″ range, we obtained the slope

$$s = -2.2 \pm 0.1, \quad (9)$$

i.e., the coma of January 1990 is significantly steeper than the coma of UT 1989 September 30. Measurements of the surface brightness of Chiron are summarized in Table VI.

IV. SPECTROSCOPY

We obtained CCD spectra of Chiron in 1989 (with the KPNO 2.1 m) and 1990 (with the CFHT 3.6 m), almost exactly 1 yr apart. The two sets of spectra were reduced in exactly the same way and divided by the same solar analog (Hyades 64) to calculate the reflectivity gradient. Division by the solar spectrum removes solar absorption lines from

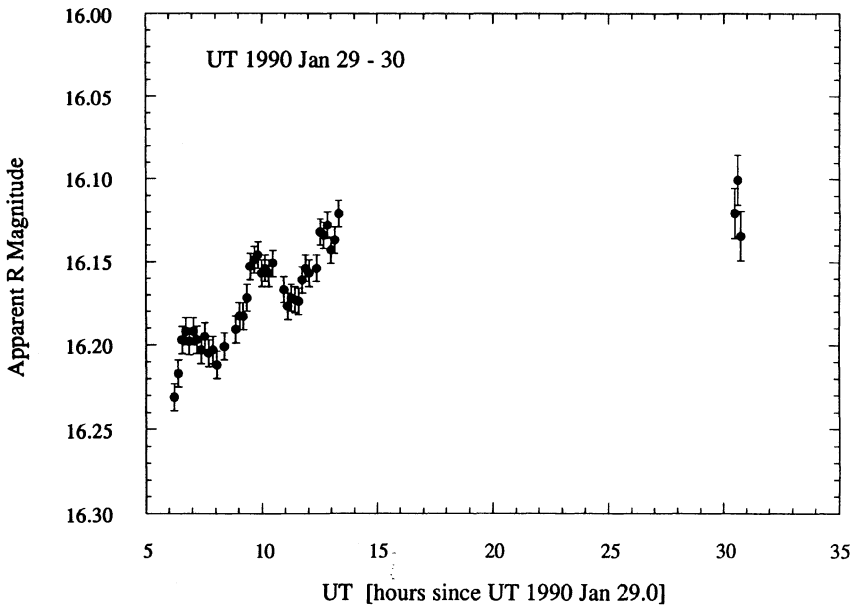

FIG. 7. Photometry from UT 1990 January 29 and 30. The brightening trend detected on the former night has decreased by the second night.

the Chiron spectra, leaving only the slope of the spectra and any discrete absorption or emission features that may be present. Treating the spectra from the 2 yr in an identical fashion allows us to compare the spectra to search for evidence for change associated with the recent cometary activity.

A useful quantity often employed in comparing reflectivity spectra of solar system bodies is the reflectivity gradient $dS/d\lambda$, i.e., the color of the spectrum. To measure $dS/d\lambda$, least-squares fits to the slope of the reflectivity are computed. The normalized reflectivity gradient S' between λ_1 and λ_2 is defined by

TABLE VII. Narrowband photometry of 2060 Chiron.

UT Date	UT hr	λ_c (Å)[a]	$\Delta\lambda$ (Å)[b]	$m \pm \sigma_m$ (mag)[c]
1990 January 30	6.8839	3200	50	18.79 ± 0.22
1990 January 30	7.0481	3200	50	18.65 ± 0.22
1990 January 30	7.4183	3200	50	18.35 ± 0.22
1990 January 30	8.2481	3650	80	18.20 ± 0.06
1990 January 30	9.0611	3650	80	18.32 ± 0.06
1990 January 30	9.2503	3871	50	18.16 ± 0.08
1990 January 30	9.4319	3871	50	18.00 ± 0.08
1990 January 30	9.6203	4060	70	17.35 ± 0.04
1990 January 30	9.8111	4060	70	17.42 ± 0.04
1990 January 30	10.0214	4260	65	17.30 ± 0.03
1990 January 30	10.2100	4260	65	17.24 ± 0.03
1990 January 30	10.3989	4845	65	16.81 ± 0.01
1990 January 30	10.5803	4845	65	16.79 ± 0.01
1990 January 30	10.7697	5139	90	16.67 ± 0.03
1990 January 30	10.8964	5139	90	16.63 ± 0.03
1990 January 30	8.6475	6840	90	16.32 ± 0.01
1990 January 30	8.8464	6840	90	16.33 ± 0.01

[a] Central wavelength.
[b] Full Width at Half Maximum transmission.
[c] In magnitude system defined by Massey *et al.* (1988).

$$S'(\lambda_1,\lambda_2) = (dS/d\lambda)/S_{6000}, \quad (10)$$

where $dS/d\lambda$ is the rate of change of the reflectivity with respect to wavelength in the range $\lambda_1 \leqslant \lambda \leqslant \lambda_2$, and S_{6000} is the reflectivity at $\lambda = 6000$ Å. Normalization at $\lambda = 6000$ Å is convenient since this is approximately the center of our wavelength range. Furthermore, our spectral range spans roughly the V and R filter bandpasses, rendering S' the spectral counterpart of the m_V-m_R color index. m_V-m_R can be found from S' by the relation

$$m_V - m_R = 2.5 \log\left[\frac{(2 + S'\Delta\lambda)}{(2 - S'\Delta\lambda)}\right], \quad (11)$$

where S' is expressed in $\%/10^3$ Å, $\Delta\lambda = \lambda_2 - \lambda_1$ is the difference in the effective wavelengths (in 10^3 Å), and $m_V - m_R$ is the object color minus the solar color (in mag).

a) February 1989 (R = 11.94–11.95 AU)

CCD spectra of Chiron were obtained on two separate nights (UT 1989 February 4 and 8) with the GoldCam (see Table III for details). An unsmoothed reflectivity spectrum of Chiron from UT 1989 February 4 is shown in Fig. 11(a). The spectrum has signal to noise $\geqslant 50$ per pixel over most of the wavelength range, the noise being higher at the shortest wavelengths (< 4000 Å) due to the decreasing transmission of the optics. The spectrum is smooth and mostly neutral, but exhibits a slight absorption feature at $\lambda \sim 4250$ Å. The absorption feature appears shallow and is ~ 400 Å wide. Its presence causes a distinct change in slope at 4600 Å; thus we fit the spectrum in two separate regions to obtain the reflectivity gradients $S'(3700, 4600)$ and $S'(4600, 7400)$. At the blue end of the spectrum, the slope is slightly positive, and $S'(3700, 4600) = 1.2\%/10^3$ Å; beyond 4600 Å, the gradient changes from positive to negative, $S'(4600, 7400) = -2.9\%/10^3$ Å. Although to a lesser extent, the same spectral trend also appears in independent spectra taken on UT 1989 February 8 [see Fig. 11(b)], which give $S'(3700, 4600) = 1.9\%/10^3$ Å, and $S'(4600, 7400) = -1.4\%/10^3$ Å. The absorption feature mentioned above is not present in

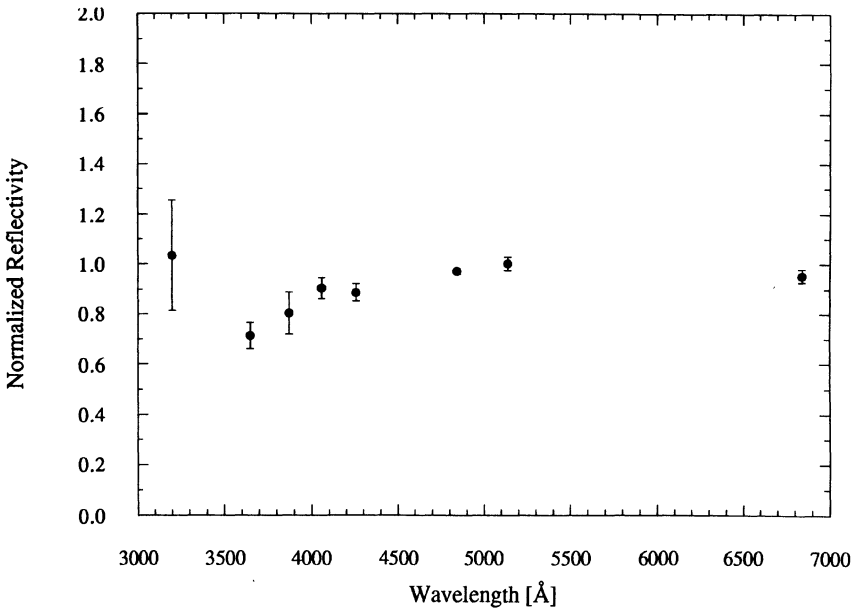

FIG. 8. Narrowband filter photometry obtained UT 1990 January 30. The photometry has been converted to reflectivity by dividing by the Arvesen *et al.* (1969) solar spectrum, and normalizing to the measurement at 5139 Å.

spectra of other objects taken in the same night (see Luu and Jewitt 1990; Jewitt and Luu 1990), and thus is unlikely to be an instrumental artifact. The spectrum of Chiron in February 1989 is thus characterized by the following two slopes:

$$S'(3700, 4600) = 1.6 \pm 0.5\%/10^3 \text{ Å}, \ 3700 \leqslant \lambda \leqslant 4600 \text{ Å}$$

and

$$S'(4600, 7400) = -2.2 \pm 0.5\%/10^3 \text{ Å}, \ 4600 \leqslant \lambda \leqslant 7400 \text{ Å}. \quad (12)$$

b) February 1990 (R = 11.25 AU)

Spectra of Chiron were obtained at the CFHT on two separate nights with different wavelength coverages: 4460 Å $\leqslant \lambda \leqslant$ 6150 Å on UT 1990 February 4 and 3650 Å $\leqslant \lambda \leqslant$ 5240 Å on UT 1990 February 5. These spectra had improved resolution over the 1989 spectra (the 1990 resolution is 10 Å FWHM, as opposed to 20 Å FWHM in 1989), as a result of a deliberate attempt to detect gaseous emissions in Chiron. Unsmoothed spectra from both nights are plotted in Fig.

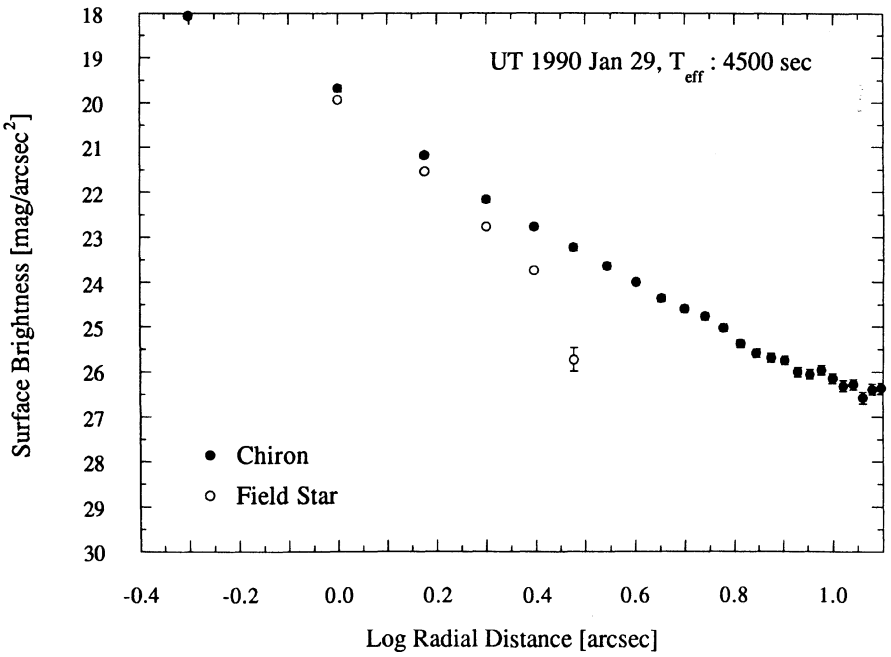

FIG. 10. Annular surface brightness profile of Chiron from a 4500 s subset of the images obtained UT 1990 January 29. Plotted error bars show the effect of a $\pm 0.5\%$ error in the determination of the surface brightness of the night sky.

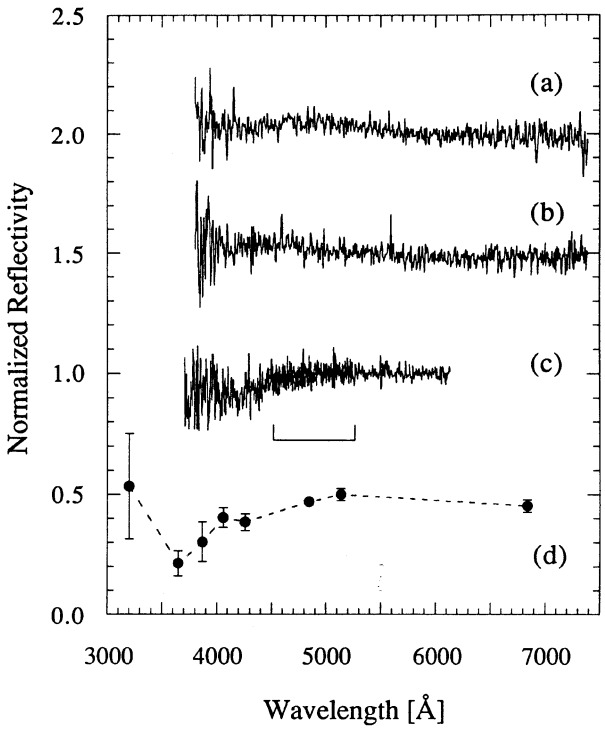

FIG. 11. Reflectivity spectra of 2060 Chiron in 1989 and 1990. Spectrum (a) is a 2000 s integration from the KPNO 2.1 m telescope obtained UT 1989 February 4, (b) is a 3600 s integration obtained UT 1989 February 8 at the same telescope. Spectrum (c) is a composite of 2 spectra (each of 2000 s) taken in February 1990 at the CFHT 3.6 m telescope (the bracket marks the region of overlap), while spectrum (d) is the narrowband filter photometry reproduced from Fig. 8. Spectra other than that from the CFHT have been shifted vertically for clarity of presentation.

11(c), where the overlapping wavelength range is marked by a bracket. The absorption feature already noticed in the 1989 spectra is again present and stronger in 1990, suggesting that it is a real and persistent feature in Chiron. The spectrum of February 1990 is characterized by the values

$$S'(3700, 4600) = 5.1 \pm 0.5\%/10^3 \text{ Å}, \ 3700 \leqslant \lambda \leqslant 4600 \text{ Å}$$

and

$$S'(4600, 5240) = 0.0 \pm 0.5\%/10^3 \text{ Å}, \ 4600 \leqslant \lambda \leqslant 5240 \text{ Å}. \quad (13)$$

The spectrum derived from the narrowband photometry is replotted in Fig. 11(d). The absorption feature at 4250 Å is again evident in the narrowband photometry, and it appears that the feature is deeper in 1990 than in either of the 1989 spectra. There is no visible evidence for gaseous emissions in the spectra. Upper limits on gaseous emissions will be discussed in Sec. VI *f*.

V. DISCUSSION

a) The Rotational Light Curve

Using the new light curve data (UT 1990 January 29) in conjunction with data from Bus *et al.* (1989), we were able to refine the rotation period of Chiron to a higher accuracy. The rotation period was previously reported as 5.9180 ± 0.0001 hr. We tested to see if this period is consistent with our light curve by correcting for light time and plotting the rotational phase of the Bus *et al.* data and of our data in Fig. 12(a). The figure shows that the light curves are similar but that there is a misalignment between corresponding peaks in the two light curves, amounting to about 0.1 unit of phase. With further calculations, we find the period which yields the best correspondence between our dataset and that of Bus *et al.*,

$$P = 5.91780 \pm 0.00005 \text{ hr}. \quad (14)$$

A phase plot with this period in Fig. 12(b) emphasizes the close match between extrema in the two datasets. Equation (14) is formally consistent with the previously determined period, but has reduced uncertainty.

Figure 12(b) clearly shows the decrease in the rotational light curve range Δm_R between 1986 and 1990. What might be the cause of this decrease? Protracted observations of the rotational light curves of short period comet nuclei show that the range decreases as the strength of the near-nucleus coma increases (Jewitt and Luu 1989). The decrease is due to dilution of light scattered from the nucleus with light scattered from a surrounding optically thin coma. To examine this explanation in the particular case of Chiron, we plot the reported range of the light curve of Chiron versus the absolute magnitude (Fig. 13). We expect (and observe) that the light curve range is correlated with the absolute magnitude, with a decrease in Δm_R by a factor of about 2, corresponding to a brightening of the same order in the total light.

To further test this explanation we represent the nucleus as a prolate spheroid with axes a, b, and c ($a > b$, $b = c$), and b being the spin axis. For simplicity, the spin axis is assumed to be perpendicular to the line of sight, i.e., the nucleus is viewed equator on. Then the nucleus light curve range Δm_o is determined by the ratio of the maximum projected cross section $C_{\max} = \pi ab$ to the minimum projected cross section, $C_{\min} = \pi b^2$,

$$\Delta m_o = 2.5 \log (C_{\max}/C_{\min}) = 2.5 \log (a/b). \quad (15)$$

Now we add an optically thin coma with a cross section C_{coma}. The new range Δm_i is

$$\Delta m_i = 2.5 \log \left[\frac{(C_{\text{coma}} + C_{\max})}{(C_{\text{coma}} + C_{\min})} \right]. \quad (16)$$

We define $k \equiv C_{\text{coma}}/C_{\max}$, and rewrite Eq. (16) in terms of k,

$$\Delta m_i = 2.5 \log\{(k+1)/[k + (b/a)]\}. \quad (17)$$

But we can express k as a function of measurable quantities such as the bare nucleus magnitude m_o and the coma-contaminated magnitude m_i,

$$k = 10^{0.4(m_o - m_i)} - 1. \quad (18)$$

Substituting Eq. (18) for k in Eq. (17), we obtain

$$\Delta m_i = m_o - m_i - 2.5 \log(10^{0.4(m_o - m_i)} + 10^{-0.4(\Delta m_o)} - 1). \quad (19)$$

We adopt $m_o = 6.24$ and $\Delta m_o = 0.09$ (from Bus *et al.* 1990), and plot Eq. (19) against the observations in Fig. 13 (the solid line). Within the uncertainties, the model is consistent with the data points, showing that the data can be explained by dilution of the light curve by an optically thin coma. For comparison, a uniformly optically thick coma would lead to a featureless light curve, since the underlying

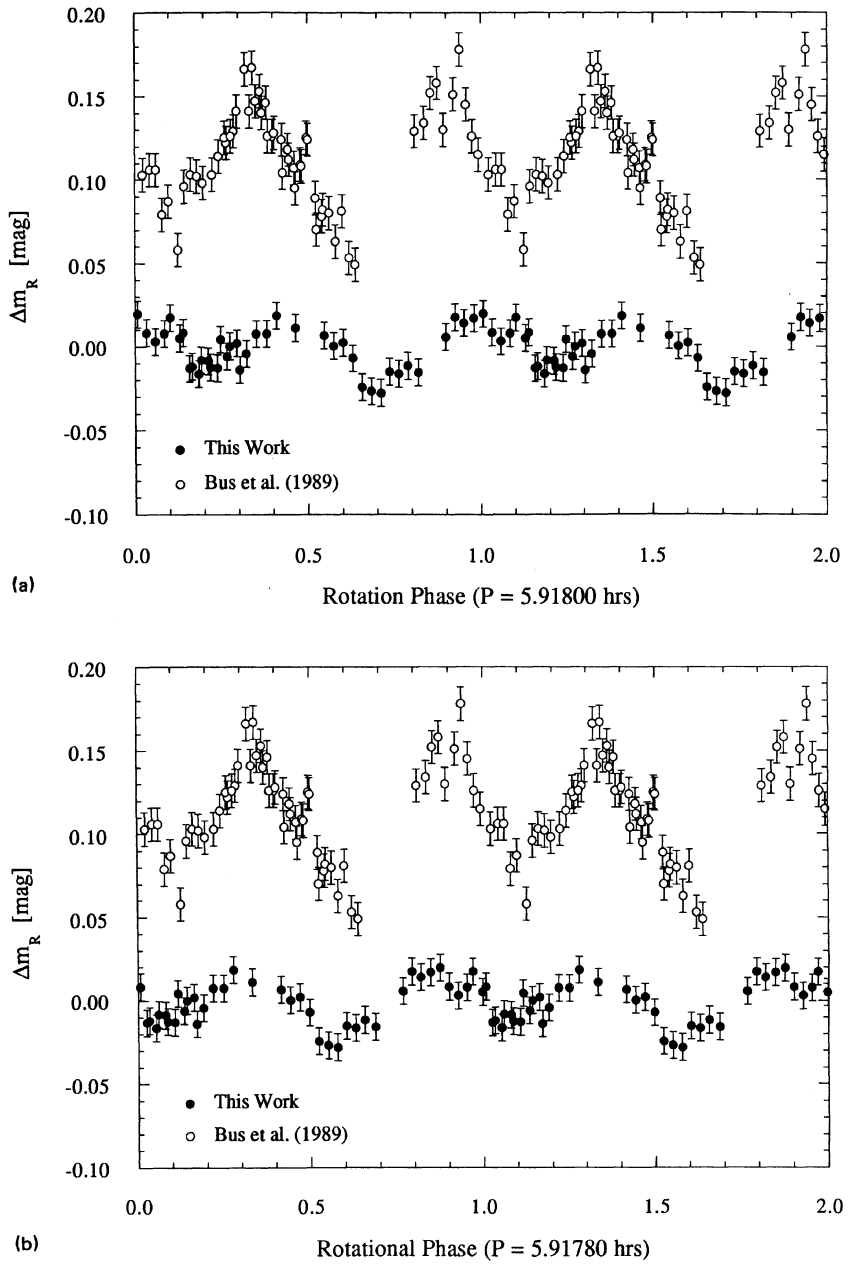

FIG. 12. (a) Rotational light curves from Bus *et al.* (1989) and from this work, reduced to rotational phase using assumed rotation period $P = 5.91800$ hr. The Bus *et al.* light curve has been displaced vertically by 0.1 mag for clarity of presentation. Note the imperfect alignment of corresponding peaks in the two light curves. (b) Same as (a) but reduced to rotational phase assuming rotation period $P = 5.91780$ hr. Corresponding peaks now appear well aligned. Note the larger range of variation in the Bus *et al.* data.

nucleus would be invisible through such a coma. Independent of the observations, we would expect the coma to be optically thin based on simple physical grounds: an optically thick coma would shield the sublimating surface from solar heating, thus reducing the temperature and cometary activity, and leading to a decrease in the optical depth.

b) The Coma

We wish to determine the source of the resolved coma of Chiron. At $R = 10$–12 AU, the sublimation rate of the dominant cometary volatile, water, is effectively zero. The second and third most abundant volatiles in comet Halley were CO ($\leqslant 16\%$) and CO_2 (3%), respectively (Festou *et al.* 1986; Krankowsky *et al.* 1986). Both molecules are candidates for the cometary activity seen in Chiron, since both are volatile at temperatures appropriate to the large heliocentric distance of Chiron at the time of its recent activity. Therefore, we investigate the nature of mass loss from Chiron driven by sublimation of CO and CO_2. Other strongly volatile substances may exist in the outer solar system (for example, nitrogen as is expected on Triton), and we emphasize that no direct evidence exists for any particular volatile on Chiron.

From Table II of Hartmann *et al.* (1990), the faintest absolute magnitude (assumed to be representative of the nucleus of Chiron) is $H_R = 6.5$ mag (see also Fig. 1), which would yield the nucleus radius $r_n = 1.2 \times 10^5$ m if the albedo is $p = 0.05$, the typical geometric albedo for the nuclei studied to date (A'Hearn 1988). This estimate of r_n is quite uncertain, since the albedo is not well known (Lebofsky *et al.* 1984 claimed a value between 6% and 20%), and since we cannot be sure that the faint state represents the complete absence of cometary activity in Chiron. However, a factor of

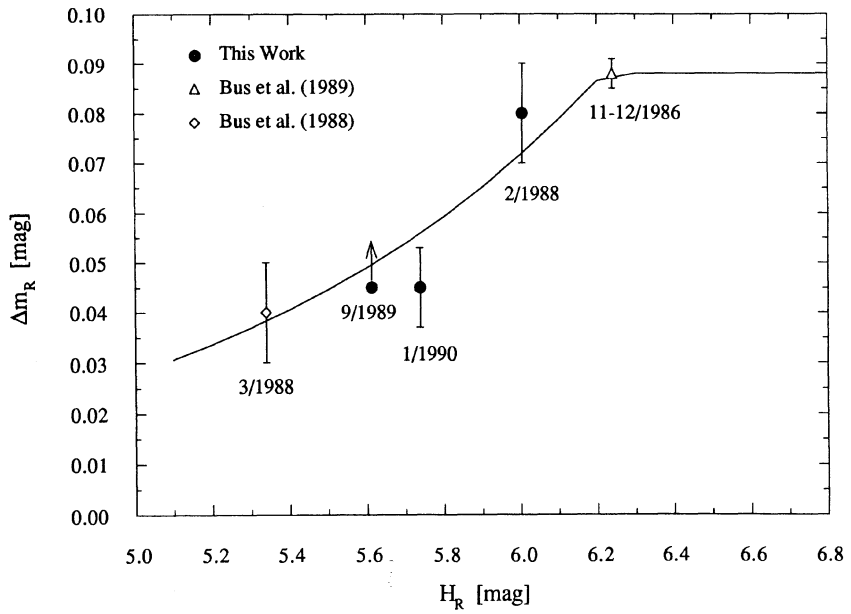

FIG. 13. Range of the rotational light curve (in magnitudes) plotted vs the mean absolute magnitude expressed in the system adopted by IAU Commission 20. Points symbolize data from dates as marked. The point from September 1989 is a lower limit. The line is the optically thin coma model discussed in Sec. V*a*.

2 error in the radius will not affect the analysis below. The gravitational escape speed from the surface of Chiron v_{esc} is 90 m s^{-1} for an assumed bulk density $\rho_n = 10^3$ kg m^{-3} and radius $r_n = 120$ km. The speed of sound appropriate to the subsolar temperature on Chiron at $R = 12$ AU is of order 160 m s^{-1} for CO and slightly larger for CO_2. Thus, gas liberated on the sunlit surface of Chiron by sublimation is not gravitationally bound, and will escape directly into space. This conclusion holds even in the extreme case in which the nucleus density is (rather arbitrarily) doubled to $\rho_n = 2\times10^3$ kg m^{-3} and the radius is doubled to $r_n = 2.4\times10^5$ m. In this sense, Chiron behaves similarly to comets of more modest size (radii $\sim$10 km), and its large presumed mass is insufficient to retain a gravitationally bound gaseous atmosphere. The escaping gases will carry entrained particles of dust away from the nucleus, so producing the resolved coma seen in Fig. 9.

How large are the particles in the resolved coma? The size of the largest particles is constrained by a balance between the force due to gas drag and the weight of the particles. The force balance equation for a spherical grain located at the equator of a spherical nucleus of radius r_n and rotating with period P is

$$\frac{d^2r}{dt^2} = \frac{3C_D N_1(R) v_{th}^2 \mu \mathscr{M}_H}{4\rho a} - \frac{4}{3}\pi G \rho_n r_n + \frac{4\pi^2 r_n}{P^2}, \tag{20}$$

where $C_D \sim 1$ is the gas drag coefficient, a is the particle radius, $N_1(R)$ is the number density due to sublimation at heliocentric distance R, v_{th} is the thermal speed of the gas, μ is the atomic weight, $\mathscr{M}_H$ is the mass of the hydrogen atom, G is the gravitational constant, and ρ_n is the density of the nucleus. The solution to Eq. (20) with $d^2r/dt^2 = 0$ gives the radius of the largest particle which can just be lifted from the surface of Chiron by gas drag. In Fig. 14, we plot (with continuous lines) the solution to Eq. (20) as a function of heliocentric distance using appropriate parameters for Chiron ($p = 0.05$, $r_n = 120$ km, $\rho_n = 1000$ kg m^{-3}, $P = 5.9178$ hr). The gas flux and the resulting $N_1(R)$ were computed from a steady-state energy balance equation applied to the sublimating surface, using the latent heats and vapor pressures for CO and CO_2 as tabulated in Cowan and A'Hearn (1982). For reference, the sublimating gas fluxes of CO and CO_2 at $R = 12$ AU are 2×10^{20} m^{-2} s^{-1} and 3×10^{17} m^{-2} s^{-1}, respectively, corresponding to $N_1(R) = 1.4\times10^{18}$ m^{-3} for CO and $N_1(R) = 1.6\times10^{15}$ m^{-3} for CO_2. The dashed lines in Fig. 14 show the effect of arbitrarily doubling the nucleus density and radius for the CO and CO_2 models. The figure shows that at $R \sim 12$ AU, particles with radii up to $a \sim 100$ (10) μm can be ejected by gas drag due to CO(CO_2) against the gravity of the nucleus. Thus, a practical upper limit to the size of the coma grains may be set at $a_{max} \sim 100$ μm if CO is the dominant volatile and $a_{max} = 10$ μm if it is CO_2. Figure 14 also shows that a_{max} is uncertain by an order of magnitude, due to uncertainties in the dimensions and density of the nucleus of Chiron. Presumably, there is no effective lower limit to the size of the grains in the coma, since all grains smaller than a_{max} can be ejected from the nucleus by gas drag. A practical lower limit on the size of the grains which contribute to the optical signature of the coma may be set at $a_{min} \sim 0.001$ μm (smaller grains approach molecular dimensions and their optical properties cannot be treated by Mie Theory). We infer that the resolved coma contains a distribution of grains with sizes in the range 10^{-9} m$\leqslant a \leqslant 10^{-4}$ m if CO is the driving volatile and $10^{-9} \leqslant a \leqslant 10^{-5}$ m if it is CO_2.

The apparent mean size of the coma grains determined from the scattered radiation is given by

$$\bar{a} = \frac{\int_{a-}^{a+} aQ_s(a,\lambda,m)\pi a^2 n(a)da}{\int_{a-}^{a+} Q_s(a,\lambda,m)\pi a^2 n(a)da}, \tag{21}$$

where $Q_s(a,\lambda,m)$ is the scattering efficiency at wavelength λ for a material of complex refractive index m, and $n(a)da$ is

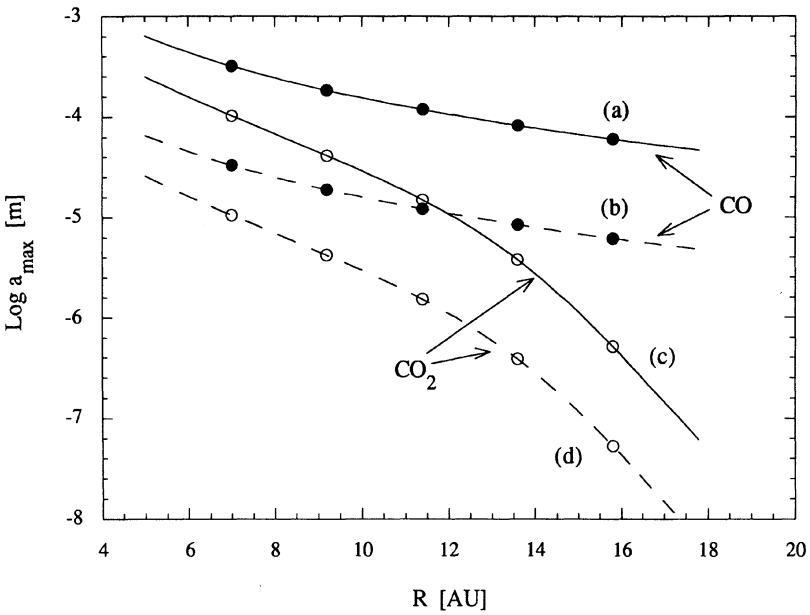

FIG. 14. The logarithm of the radius (in meters) of the largest particle which can be ejected from the surface of Chiron by gas drag is plotted against the heliocentric distance (AU). (a) The curve was computed from Eq. (20) for CO ice in equilibrium sublimation, using parameters as described in Sec. V *b*, and assuming a Chiron radius $r_n = 120$ km and nucleus density $\rho_n = 1000$ kg m^{-3}; (b) same as (a) but assuming $r_n = 240$ km, $\rho_n = 2000$ kg m^{-3}; (c) same as (a) but for CO_2 ice in equilibrium sublimation; and (d) same as (c) but assuming $r_n = 240$ km, $\rho_n = 2000$ kg m^{-3}.

the number of grains having radii in the range a to $a + da$. In comets, $n(a)da$ is approximated by an inverse cubic or inverse quartic power law (Lamy, Grün, and Perrin 1987). In practice, it is found that observations at wavelength λ are biased towards particles with radii $a \sim \lambda$, since grains with $a \ll \lambda$ are poor scatterers [$Q_s(a,\lambda,m) \ll 1$] while grains with $a \gg \lambda$ are rare. This finding is supported by detailed evaluation of Eq. (21), using Mie theory to compute $Q_s(a,\lambda,m)$. For definiteness, we adopt $\bar{a} = 1$ μm as the effective grain size in our optical data, while recognizing that smaller and larger grains may exist in the coma. Our subsequent conclusions are not strongly dependent on the choice of $\bar{a}$.

The optically dominant $\bar{a} \sim 1$ μm particles would be dynamically well coupled to the strong gas flow due to sublimation of CO, and would leave the nucleus at a large fraction of the gas velocity. We adopt $u \sim 100$ m s^{-1}, as a rough estimate of their terminal velocity. The same particles would leave at near zero terminal velocity if the activity were instead driven by CO_2. Particles of micron size are strongly influenced by radiation pressure (Burns, Lamy, and Soter 1979; Lamy and Perrin 1988). Thus, we expect that the coma of Chiron should show morphological effects indicative of the action of radiation pressure. Specifically, we expect that the coma should be asymmetrical, with a tail of small particles extending in the antisolar direction. The existence of a tail is difficult to confirm using available observations, since the comet is observed at very small phase angles ($\alpha < 4°$) and foreshortening is very great [the projection factor is $1/\sin(\alpha) \geqslant 14$]. No tail is obvious in our data (Fig. 9), although it was noted in Sec. III *d* that the coma *is* elongated in the antisolar direction, compatible with radiation pressure.

We estimate the time for radiation pressure to sweep particles through the observed coma as follows. The apparent radius of the coma in the plane of the sky in January 1990 is $\sim 10''$ (see Fig. 9), corresponding to $L \sim 8 \times 10^7$ m at the comet. Including the projection factor, the true length in the antisolar direction must be of order $L' = L/\sin(\alpha)$ $\sim 1.9 \times 10^9$ m. If dust particles are ejected from the sunlit side of the nucleus at a sunward velocity $u \sim 100$ m s^{-1}, the time needed for radiation pressure to deflect a grain down the tail through a distance L' is

$$\tau_r = (u + \sqrt{u^2 + 2\beta g_{\rm Sun} L'})/\beta g_{\rm Sun}, \qquad (22)$$

where $\beta \sim 0.2$ is the appropriate radiation pressure factor (Burns, Lamy, and Soter 1979) and $g_{\rm Sun} = 4 \times 10^{-5}$ m s^{-2} is the local solar gravitational acceleration. Substituting the appropriate values, we obtain

$$\tau_r \sim 3 \times 10^7 \text{ s}, \qquad (23)$$

or about 1 yr. Equation (23) constitutes a useful lower limit to the time of residence of micron-sized grains in the coma. It is a *lower* limit since very large and very small grains will be less affected by radiation pressure than the optically important $a \sim 1$ μm grains, and will take longer to leave the coma.

We believe that the long residence time given by Eq. (23) provides a simple and natural explanation for the long duration of the "outburst" plotted in Fig. 1. In particular, Eq. (23) shows that even if the source of the coma particles were suddenly to cease, the resolved coma would remain populated with grains for a time of order 1 yr. From the figure, Chiron has experienced a steady increase in brightness since mid-1987, and the trend has turned into a decrease in brightness since early 1989. The slow decline in the total magnitude witnessed since early 1989 (Fig. 1) can be reasonably attributed to the long residence time of typical particles in the visible coma. At any instant t, the observed coma consists of the sum of all the particles ejected from the nucleus between t and $t - \tau_r$. Thus a very weak but persistent source of escaping particles could populate the observed coma of Chiron on a timescale of order 1 yr. A weak but persistent source would be compatible with the nondetection of coma in Chiron until 1–1.5 years after the start of the photometric outburst.

Given that the coma is optically thin and that the effective mean radius of the scatterers is $\bar{a} \sim 1$ μm, the mass of the

coma may be directly estimated from the photometry (c.f., Jewitt 1990b). The mass $\mathscr{M}$ of an ensemble of particles with radius a and total cross section C is $\mathscr{M} \sim fpaC$, where f is a numerical factor of order unity determined by the form of the grain size distribution, and $\rho = 1000$ kg m^{-3} is the grain mass density. The grain cross section estimated from the integrated CCD photometry is $C \sim 1.4 \times 10^{10}$ m^2. Substituting, we obtain $\mathscr{M} \sim 1.4 \times 10^7$ kg as the total grain mass. The estimate is good only to an order of magnitude, since, as noted previously, the effective grain radius is known to this order. If the coma were ejected uniformly over a 1 yr period, the derived mean mass loss rate in grains is 0.4 kg s^{-1}. Note that our detection of impulsive brightening shows that the instantaneous mass loss rate may be 2 orders of magnitude larger than the mean value. In any case, the observed coma is compatible with very small masses of dust ejected at low rates. For reference, the specific rates of equilibrium sublimation of CO and CO_2 are estimated as 1.1×10^{-5} and 6.8×10^{-8} kg m^{-2} s^{-1}, respectively. Exposed volatile areas as little as $A(CO) = 3.6 \times 10^4$ m^2 (0.04 km^2) and $A(CO_2) = 5.9 \times 10^6$ m^2 (6 km^2), corresponding to 10^{-5} to 10^{-7} of the surface area of a ~ 120 km radius nucleus, could produce the observed mean mass loss rate averaged over 1 yr. The estimated coma mass corresponds to a volume $V \sim 1.4 \times 10^4$ m^3, if the bulk density $\rho = 10^3$ kg m^{-3} is assumed for the coma particles. Including a comparable mass of CO or CO_2 ice, we estimate that a total volume $V \sim 3 \times 10^4$ m^3 has been ejected into the coma. If CO is the driving volatile, the depth of excavation would be $V/A \sim 0.8$ m, and $V/A \sim 5 \times 10^{-3}$ m (5 mm) if CO_2 is responsible. Thus, activity in Chiron may be confined to a very thin layer near the surface.

Whereas particles with radii up to a few tens to a hundred microns (depending on the active volatile and the nucleus parameters) will eventually escape from Chiron, a different fate must await larger particles. Such particles are presumably ejected from the surface of Chiron by gas drag, but fail to achieve escape speed. These particles must enter ballistic trajectories about Chiron, presumably reimpacting the surface shortly after release. Banaszkiewicz *et al.* (1990) have shown by numerical integration of the equations of motion that grains can follow complicated paths when ejected from a rotating, aspherical nucleus at a speed comparable to the escape speed. On the basis of their calculations, we expect that a short-lived, gravitationally bound coma of grains might exist around the nucleus of Chiron. The scale of this bound coma ($\leqslant 10$ Chiron radii) would be small compared to the typical angular resolution of our Mauna Kea data, and it can have no contribution to the extended coma seen in Figs. 2, 5, 9, and 10. However, the bound coma could add light to the core of the Chiron images, without contributing to the wings. Therefore, it is worthwhile to examine the surface brightness profiles of Chiron for evidence of a near-nucleus, bound coma.

c) The Nucleus and the Bound Coma

An empirical upper limit to the fraction of the coma cross section which is gravitationally bound can be obtained from the surface brightness profiles discussed earlier. The components that contribute to the integrated magnitude of Chiron are the bare nucleus, the bound (unresolved) coma, and the unbound (resolved) coma. Ideally, we would use the profiles of field stars to deconvolve the profile of Chiron into its separate components. In practice, deconvolution tends to amplify noise in the data, and we obtain results of greater physical value by performing the reverse process, i.e., by convolving idealized models with the seeing profile. We make use of a convolution model to fit the resolved coma and to extrapolate to the center of the coma, thereby yielding the magnitude of the unresolved core. A brief description of this method can be found in Luu and Jewitt (1989); it is described in fuller detail in Luu (1990). The essence of the method is to convolve model comae with the seeing and to fit the convolved model comae to the observed profile. The seeing is sampled directly from the data in the form of the point-spread function of field stars. The preconvolved model of Chiron consists of a power law surface brightness coma $B(r) \alpha r^s$, with a central "spike" added to represent the sum of the nucleus and any bound coma. The profiles in Sec. III suggest indices in the range $-1.5 \geqslant s \geqslant -2.2$. For any value of s, each model profile is parametrized by a quantity $\mathscr{R}$, defined as the ratio of the cross section of the unbound coma measured in a 1″ radius aperture C_{unbound} to the resolved core cross section $C_{\text{nuc}} + C_{\text{bound}}$,

$$\mathscr{R} \equiv C_{\text{unbound}} / (C_{\text{nuc}} + C_{\text{bound}}). \quad (24)$$

A set of models having different $\mathscr{R}$ and s are computed and fitted to the observed profile.

We discuss the profile of Chiron taken from a single image of UT 1990 January 29. In Fig. 15(a), we show the Chiron profile and the profile of a nearby star, and a close-up view is provided in the enclosed box. Chiron is clearly broader than the star, with the coma most apparent in the wings of the profile. By fitting various model profiles to the observed profile, we find that the model with $s = -2$ and $\mathscr{R} = 0.5$ provides the best fit. In Fig. 15(b), we show profiles of Chiron and of the best fitting model ($s = -2$ and $\mathscr{R} = 0.5$), and a close-up view of the profile wings shows clearly that the fit is a good one. From $\mathscr{R}$, we can subtract the coma contribution from the integrated magnitude (within 1″ radius), to find the mean absolute magnitude of the nucleus and the bound coma $\overline{H_R}_{(\text{nuc + bound coma})}$,

$$\overline{H_R}_{(\text{nuc + bound coma})} = 6.35 \text{ mag}. \quad (25)$$

Equation (25) is consistent with the faintest measurements of Chiron, obtained in late 1982 and early 1983 (Fig. 1), when the object $\overline{H_R} = 6.3$–6.5 mag. We therefore conclude that the contribution from the bound coma could not exceed ~ 0.1–0.2 mag (10%–20%) in January 1990. The evidence therefore suggests that the bound coma is not a photometrically important entity in Chiron, at least not in January 1990.

d) Surface Brightness Profiles

In the absence of radiation pressure, an isotropic, steady-state dust coma would have a surface brightness profile $B(r) \alpha r^s$, with $s = -1$. Inclusion of radiation pressure steepens the profile towards a limiting case given by $s = -1.5$ (Jewitt 1990b). In Chiron, the surface brightness profile had a gradient very close to the limiting radiation pressure case in September 1989 [Eq. (5)], but substantially steeper in January 1990 [Eq. (9)]. How can the steep surface brightness profile of Chiron in early 1990 be explained?

A simple and natural explanation may be given in terms of the combined effects of radiation pressure and intrinsic variability of the activity on Chiron. In addition to the year-long increase in the total magnitude, we have already noted the existence of short-duration brightenings ("outbursts"),

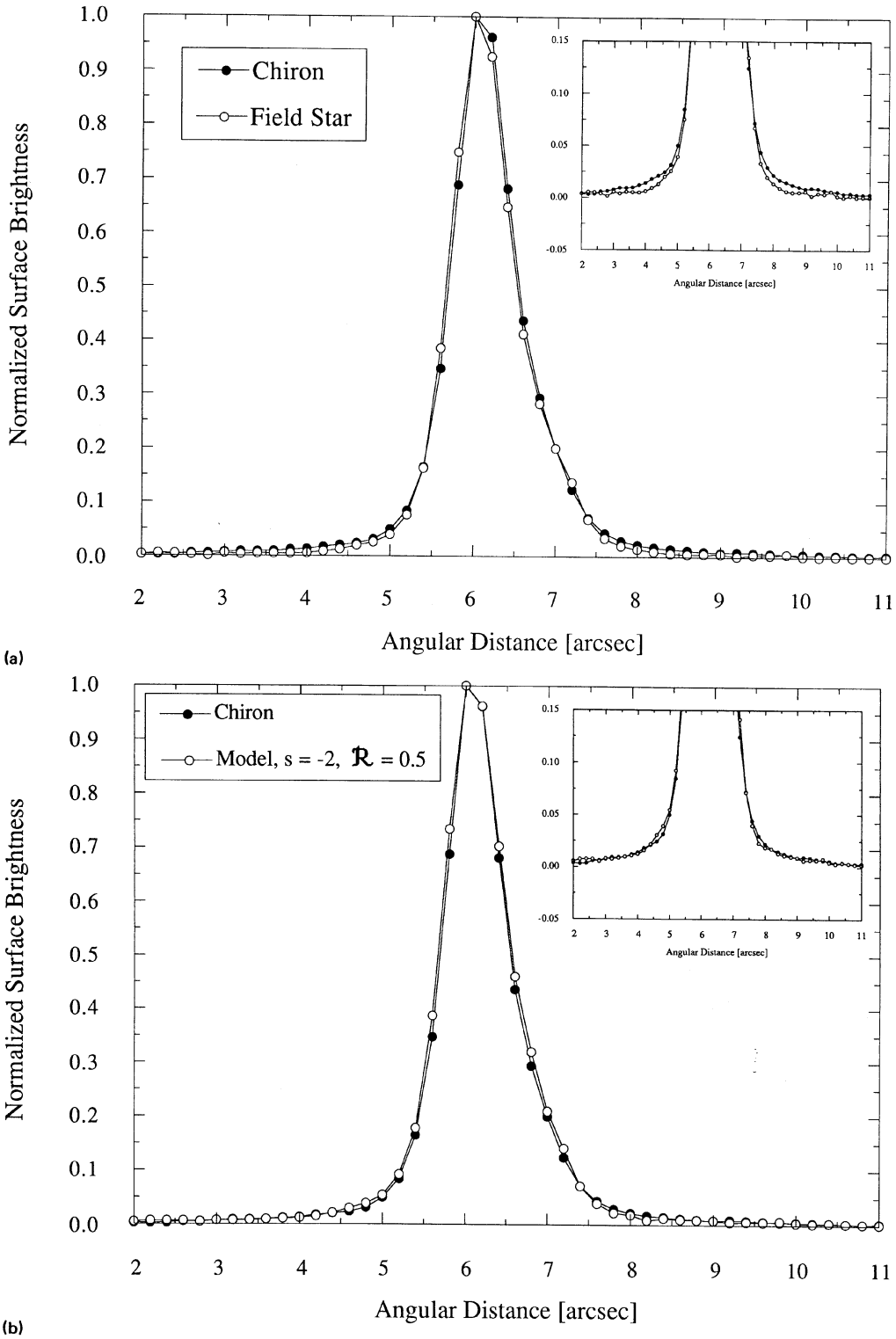

FIG. 15. (a) Linear profiles of Chiron and a field star from an observation taken on UT 1990 January 29. The profiles were determined from cuts made perpendicularly to the projected motion of Chiron. The enclosed box provides a close-up view of the wings of the profiles, where the difference is most significant. The profile of Chiron is clearly broader than that of the star. (b) Linear profiles of Chiron and of a model comet. The model is characterized by a coma which obeys a power law surface brightness (index $s = -2$), and by the parameter $\mathscr{R} = 0.5$, where $\mathscr{R}$ is defined by Eq. (24) in the text. The enclosed box provides a close-up view of the wings of the profiles and the model [cf. Fig. 15(a)].

with rates up to 15 millimag/hr (Sec. III *d*). By comparison, the mean rate of brightening during the year-long outburst starting from 1987 to 1988 is of order 1 mag/1 yr $\sim$0.1 millimag/hr. Evidently, the instantaneous rate of mass loss from Chiron can exceed the mean rate by a factor of 150, suggesting that the mass loss is intrinsically impulsive in nature and superimposed upon steady-state sublimation. In retrospect, supporting evidence for this conclusion is obvious in Fig. 1, where it may be seen that the scatter in the mean magnitude at any epoch is large compared to the uncertainties in the photometry. Evidently, the photometry in Fig. 1 significantly undersamples short-term variations in the total light resulting from impulsive activity on the nucleus. Therefore, the assumption of steady-state coma formation is not valid in

the case of Chiron over short timescales. The causes of the impulsive outbursts of Chiron are not known. One possible explanation is the activation and depletion of volatile pockets on the surface. New volatile pockets could be activated in a random manner simply by increased solar heating, or they could be exposed by gravity-induced redistribution of material on the surface. Downslope movement of material has been observed on the satellite Deimos, an object merely 6 km in radius (Thomas and Veverka 1980). Similar downslope movement on Chiron could be initiated by infall of large suborbital grains ejected from active sites near the subsolar point. However, we emphasize that we have no constraints on the possible theories of cometary activity on Chiron, and the scenario mentioned above is speculative at best.

The surface brightness gradient should vary in response to the variable mass loss rate from the nucleus. A steep surface brightness gradient would result from a recent episode of activity, with the fresh grains having traveled only a short distance from the nucleus in the time since their ejection. Conversely, the gradient should become less steep in times corresponding to declining nuclear activity. Qualitatively, we expect that the surface brightness gradient should equal -1.5 (due to the effect of radiation pressure) in the periods of steady activity between impulsive ejections. The gradient should steepen following an outburst, and remain steep for a time comparable to the grain residence time τ_r. In this scenario, excess mass loss occurring between our September 1989 and January 1990 profile determinations would be responsible for the steep profile observed in the latter period. We further predict that future measurements should show fluctuations in s occurring on timescales of months to a year, and that the fluctuations should be correlated with variations in the mass loss rate.

e) Spectra: The Continuum

The reflectivity spectra shown in Fig. 11 (taken in two different years with three different instruments) show that Chiron is nearly neutral in the 4600–7400 Å range. However, shortward of 4600 Å, there exists an absorption band similar to the broad UV absorption observed in asteroids and meteorites [which is caused by charge transfer in a transition metal silicate (Gaffey, Bell, and Cruikshank, 1989, Chapman and Gaffey 1979)]. On the whole, the neutral reflectivity and the onset of the UV absorption shortward of 4600 Å bear strong resemblance to the reflectivity of typical C-type asteroids (Tholen and Barucci 1989). This result is independent of, but consistent with, the filter observations of Hartmann *et al.* (1990) at wavelengths $\lambda > 5000$ Å. The neutral reflectivity of Chiron is reminiscent of the nucleus of comet P/Halley ($S'_{\rm Halley} = 6 \pm 3\%/1000$ Å; Thomas and Keller 1989), while other known comet nuclei tend to be redder (A'Hearn 1988; Jewitt 1990b). The small database gathered thus far on comet nuclei seems to indicate that the comet nucleus population is a diverse one, and it would be premature to conclude that Chiron is spectrally unlike the nuclei of other comets.

The depth of the absorption feature shortward of 4600 Å may be time variable. The feature was very weak in 1989 [see Figs. 11(a) and 11(b)], but considerably deeper in 1990, as is evident in both the CCD spectra and narrowband filter photometry of 1990 [Figs. 11(c) and 11(d)]. The change is also apparent in the separate measurements of S' in Eqs. (12) and (13). Possibly, the absorption feature is intrinsic to the nucleus of 2060 Chiron and is absent in the coma. The change in the depth of the feature would then occur because the coma is slowly dissipating, and has faded by $\Delta m \sim 0.4$ mag in the interval between the 1989 and 1990 spectra (see Fig. 1). This scenario is consistent with the slow decline in brightness observed since early 1989 and the slow expansion velocity of the coma postulated earlier (see Sec. V *b*), and predicts that the absorption feature would appear stronger still in a spectrum of the bare nucleus of Chiron.

From Sec V *b*, we know that the particles in the coma must be small in order to escape the gravitational field of the nucleus ($a \leqslant 100\,\mu$m if CO is the dominant volatile and $\leqslant 10\,\mu$m if it is CO_2). Mie theory predicts that in the regime where $a \ll \lambda$ (the Rayleigh regime), the scattered intensity is proportional to $1/\lambda^4$ (c.f., van de Hulst 1957). It is natural to expect that submicron particles might give rise to detectable Rayleigh scattering, particularly in the CO_2 generated coma where even the largest ejected grains have $a \sim \lambda$ and a majority satisfy $a \ll \lambda$. However, Rayleigh scattering is not evident in Chiron (Fig. 11).

We investigate the lack of Rayleigh scattering in Chiron by calculating the reflectivity as a function of wavelength, using Mie theory and the refractive indices of various materials, including glassy carbon (Edoh 1983), "astronomical silicate" (Draine 1985), and tholin (Khare *et al.* 1984). The parameters used in computing the model reflectivities are the grain size range, the power law index for the size distribution, and the wavelength-dependent refractive indices for each material. The reflectivities are then added to a scaled neutral reflector (to simulate the nucleus) and normalized at $\lambda = 5139$ Å for direct comparison with the data. The narrowband spectrum of Chiron and the model spectra are plotted in Fig. 16; the models are computed with the size range $0.001 \leqslant a \leqslant 100\,\mu$m (as appropriate for CO-dominated sublimation), and the power law index $q = 3,4$. Figure 17 shows comparable models with the size range $0.001 \leqslant a \leqslant 10\,\mu$m (as appropriate for CO_2-dominated sublimation). The plotted models provide an adequate fit to the near-UV Chiron spectrum, within the uncertainties of the data. However, the main point to be noted about Figs. 16 and 17 is not which material fits the Chiron spectrum the best, but the real lack of Rayleigh scattering at short wavelengths. Although small particles are included in the size distributions and must give rise to Rayleigh scattering, their contributions to the spectra are evidently swamped by scattering from the nucleus and from larger grains in which the scattering is neutral or even reddish. This result was verified by computing models with and without a nucleus contribution. Presumably, the spectral domination by large grains also accounts for the general lack of Rayleigh scattering in cometary spectra. Thus the absence of near-UV Rayleigh scattering in the coma of Chiron imposes no useful constraints on the size of the grains, other than the obvious one that $\bar{a}$ is not $\ll \lambda$.

f) Spectra: Gaseous Emissions

As noted in Sec. V *b*, the activity in Chiron is not water based, but may instead indicate sublimation of more volatile materials such as CO or CO_2. We decided to search for evidence of CO^+ emission in Chiron since (a) CO^+ can be produced from both CO and CO_2 (e.g., Huebner and Giguere 1980), and (b) CO^+ has been reported in other distance comets [e.g., P/Schwassmann–Wachmann 1 at $R = 6.1$ AU (Cochran, Barker, and Cochran 1980), comet Humason at $R = 5$ AU (Dossin 1966)].

Our search focused on the CFHT–Herzberg spectra

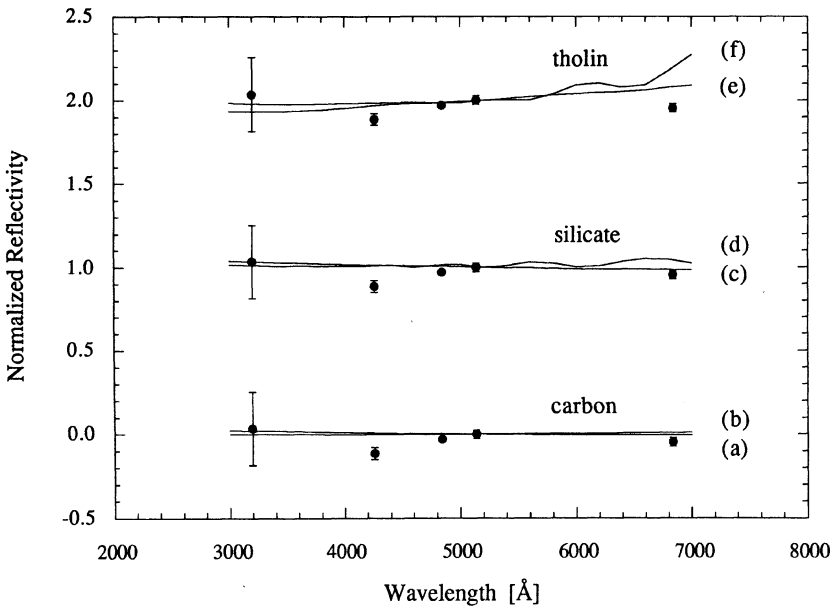

FIG. 16. Reflectivity spectra of Chiron and Mie models computed with complex refractive indices for "glassy carbon," "astronomical silicate," and "tholin;" the size range used in all models is 0.001 $\mu m \leqslant a \leqslant 100$ μm. For ease in comparison, the spectra of each material are arbitrarily offset and the spectrum of Chiron is replotted with each material. (a) carbon, $q = 4$, (b) carbon, $q = 3$, (c) silicate, $q = 4$, (d) silicate, $q = 3$, (e) tholin, $q = 4$, and (f) tholin, $q = 3$.

shown in Fig. 11(c). Special practical considerations are needed to search effectively for molecular bands in comets at large distances. Molecules released from the nucleus photodecay at rates characteristic of the molecule and of the heliocentric distance. At $R = 1$ AU, for instance, typical decay scale lengths for prominent molecules are $D \sim 5 \times 10^7$ m (A'Hearn 1982). When observed from a distance $\Delta \sim 1$ AU, the decay length subtends an angle $D/\Delta \sim 60''$. For photon destruction, the decay length scales in proportion to R^2, while the subtended angle scales as R^2/Δ. Thus, the same molecule observed in a comet at $R \sim 10$ AU would have an angular decay scale $\sim 600''$. Spectra taken to search for cometary emission in distant comets cannot employ local sky subtraction, since molecular features would tend to be self subtracted. For this reason, we obtained sky spectra separated from Chiron by 600″ in the plane of the sky, and used these spectra for the sky subtraction in our search for molecular features.

Our search concentrated on the $A\,^2\Pi_i - X\,^2\Sigma^+$ transitions of CO^+ at 4000 Å ($\Delta\lambda \sim 50$ Å) and 4260 Å ($\Delta\lambda \sim 60$ Å) (Wyckoff 1982; Wyckoff and Wehinger 1976). Careful examination of the spectra taken on UT 1990 February 5 showed no evidence for gaseous emission at these wavelengths; in fact, no emission feature could be seen throughout the covered spectral range. From the spectra, we measured 3σ upper limits for the CO^+ flux densities in bands centered on 4000 and 4260 Å, and calculated the column density, assuming the g factor for resonance fluorescence

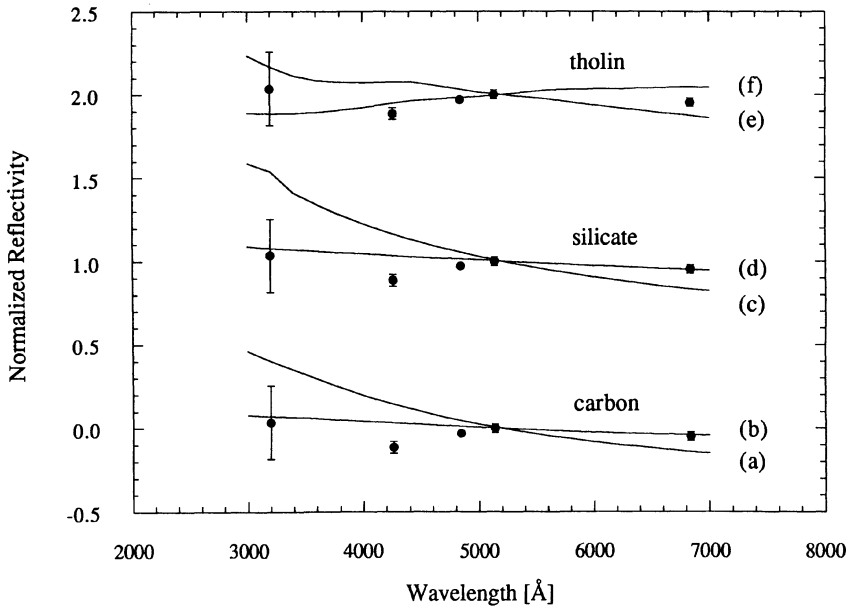

FIG. 17. Same as Fig. 16, but with the size range 0.001 $\mu m \leqslant a \leqslant 10$ μm. (a) carbon, $q = 4$, (b) carbon, $q = 3$, (c) silicate, $q = 4$, (d) silicate, $q = 3$, (e) tholin, $q = 4$, and (f) tholin, $q = 3$.

$g = 6.2\times10^{-3}$ at $R = 1$ AU (Wyckoff and Wehinger 1976). The adopted g factor does not account for Swings' effect (i.e., it does not take into account the velocity of Chiron with respect to the Sun), but is probably correct to within a factor of 2. The 3σ upper limits for the CO^+ flux densities for the bands at 4000 and 4260 Å are 1.2×10^{-14} ergs s^{-1} cm^{-2} $Å^{-1}$ and 1.0×10^{-14} ergs s^{-1} cm^{-2} $Å^{-1}$, respectively. The two CO^+ bands give consistent column densities (they lie within 20% of each other), and we adopt the average value 6.6×10^{11} ions cm^{-2} as our 3σ upper limit for the CO^+ column density on UT 1990 February 5 ($R = 11.25$ AU). The upper limit to the total number of CO^+ ions in the slit aperture is 3.3×10^{30} ions, corresponding to $\leqslant 1.5\times10^5$ kg. The time of residence of the ions in the 1.1×10^4 km $\times 4.3\times10^4$ km aperture is $\geqslant 5.5\times10^4$ s, so that we estimate a very crude upper limit to the CO^+ production rate as 2.7 kg s^{-1}. Thus the limit to the CO^+ production rate is greater than, but on the same order as, the dust production rate (0.4 kg s^{-1}, Sec. V b).

VI. CONCLUSIONS

From 2 yr of detailed photometric and spectroscopic observations we deduce the following key observational parameters of 2060 Chiron:

(1) The photometric outburst which began in late 1987 (Hartmann *et al.* 1990) peaked at absolute red magnitude $\overline{H_R} = 5.25$ in late 1988, and has since followed a general decline. The amplitude of the outburst at its peak was 1.1 ± 0.1 mag. Typical rates of change of the absolute magnitude were 0.1 millimag/hr averaged over the year-long rise and decline portions of the outburst.

(2) Photometry obtained UT 1990 January 29 and 30 shows impulsive brightening at the much higher rate 15 millimag/hr. Thus the steady brightening over the last few years conceals a series of short-lived brightenings corresponding to episodic mass loss ("outbursts").

(3) The best estimate of the synodic period of rotation of the nucleus is $P = 5.91780 \pm 0.00005$ hr.

(4) The photometric range of the light curve is diminished in proportion to the absolute magnitude of the comet, from $\Delta m_R = 0.09$ mag in 1986 to $\Delta m_R = 0.045$ mag in 1990.

(5) The reflectivity of Chiron is optically similar to that of a C-type asteroid. Reflectivity spectra in 1989 and 1990 suggest a near-ultraviolet absorption at wavelengths $\lambda < 4600$ Å superposed on a nearly neutral spectrum at longer wavelengths. The depth of the absorption is greater in 1990 than in 1989, and may be anticorrelated with the brightness of the coma.

(6) The is no evidence for Rayleigh scattering in the reflection spectrum down to $\lambda = 3200$ Å in January 1990.

(7) The coma of Chiron is not resolved in February 1988 but is clearly resolved in September 1989 and January 1990. A 20 000 s integration from January 1990 reveals asymmetric coma in position angle $157 \pm 3°$, visible to surface brightness 26.4 ± 0.1 mag/arcsec^2 at distance 12.5″. The coma extension is in the projected antisolar direction.

(8) The coma possesses a steep but time-variable surface-brightness profile. Measurements of high-resolution imaging data yield the power index $s = -1.5 \pm 0.1$ in September 1989 and $s = -2.2 \pm 0.1$ in January 1990.

(9) There is no evidence for gaseous emissions in the $3600 \leqslant \lambda \leqslant 6200$ Å spectral range in data taken February 1990 at the Canada–France–Hawaii Telescope. The empirical upper limit on the CO^+ column density is 6.6×10^{11} ions cm^{-2}.

From these key observations and from simple physical arguments, we deduce the following portrait of cometary activity in 2060 Chiron:

(1) The production of coma in Chiron in 1987–1990 is attributed to sublimation of near-surface volatiles. Water cannot sublimate at $R > 6$ AU (as in the case of Chiron) since the surface temperatures are too low. Instead, we focus attention on CO and CO_2 as the source of the current activity, since both molecules were found in comet Halley in substantial abundance. Sublimated gas escapes directly from the (unusually large) nucleus, propelling entrained dust grains into the resolved coma.

(2) The optical mean size of the particles in the resolved coma is of order 1 μm. Larger particles, 10 μm and 100 μm, can be ejected from the nucleus by CO_2 and CO, respectively. Models of the scattering from power law size distributions of silicate, glassy carbon, and tholin grains are compatible with the empirical absence of blue colors (Rayleigh scattering) down to $\lambda = 3200$ Å.

(3) The mass of the grain coma in January 1990 is $\mathcal{M} \sim 1.4\times10^7$ kg. The time-averaged rate of mass loss in grains from the nucleus is a very modest 0.4 kg s^{-1}, although rates two orders of magnitude larger may occur in impulsive outbursts. Limits on the production rate of CO^+ determined from spectra are $\leqslant 2.7$ kg s^{-1}, similar to and consistent with the dust mass loss rates. An active area of CO as small as 0.04 km^2, or of CO_2 of 6 km^2, can supply the inferred mean mass loss rate, corresponding to 10^{-5}–10^{-7} of the surface area of $a \sim 120$ km radius nucleus.

(4) The form of the dependence of the rotational light curve range on the absolute magnitude shows that the coma of Chiron is optically thin along the line of sight to the nucleus. An optically thin coma is independently anticipated from physical considerations, since an optically thick coma would stifle further sublimation.

(5) Detailed models of the central surface brightness profiles provide no evidence for a gravitationally bound (unresolved, near-nucleus) coma of large grains. Specifically, the cross section of the bound coma is < 10–20% of the total coma cross section at its peak. Evidently, the bound coma is not a photometrically important entity in Chiron, despite the large mass and gravity of the nucleus.

(6) The long duration of the 1987–1990 photometric outburst is attributed to the large time of residence of micron-sized grains in the resolved coma. The residence time is $\tau_R \sim 1$ yr, and is determined by solar radiation pressure. Rapid brightening detected in January 1990 demonstrates that Chiron is active even though the total brightness was then decreasing.

(7) The near-ultraviolet absorption feature in the reflectivity spectrum is affected by scattering from the coma, and may become stronger as the coma of Chiron fades.

We are grateful to the CFHT and KPNO personnel for their tireless and efficient support, and we thank Yuhong Fan for her energetic assistance at the UH telescope. This work was supported by a NASA Planetary Astronomy grant to D.C.J. and a NASA Graduate Student Fellowship to J.X.L.

Note added in proof: In mid-July 1990, we received a report on 2060 Chiron by R. West (in The ESO Messenger, Vol. 60, pp. 57–59), and a preprint by K. Meech and M.

Belton (submitted to Astron. J.). The work by West parallels our own, but differs in that he finds very blue optical colors for the coma of 2060 Chiron. Our independent CCD spectra and narrowband photometry at 8 wavelengths (Fig. 11) appear inconsistent with the large blue color. However, a detailed comparison remains to be made. The work by Meech and Belton addresses a model in which the coma of Chiron is gravitationally bound. As noted above in Sec. V*c*, the surface brightness profile of Chiron suggests that the bound coma is not a photometrically important entity, in the sense that it contains less than 10–20% of the scattering cross-section.

REFERENCES

A'Hearn, M. F. (1982). In *Comets*, edited by L. Wilkening (University of Arizona Press, Tucson), pp. 433–460.

A'Hearn, M. F. (1988). In *Annual Review of Earth Planetary Science 1988*, edited by G. Wetherill, A. L. Albee, F. G. Stehli (Annual Reviews, Palo Alto), pp. 273–293.

Arvesen, J. C., Griffin, R. N., and Pearson, Jr., B. D. (1969). Appl. Opt. **8**, 2215.

Banaszkiewicz, M., Marconi, M. L., Kömle, N. I., and Ip. W.-H. (1990). In *Asteroids, Comets, Meteors III*, edited by C. I. Lagerkvist, H. Rickman, B. A. Lindblad, and M. Lindgren (Uppsala University Press, Sweden), pp. 235–238.

Bowell, E., Hapke, B., Domingue, D., Lumme, K., Peltoniemi, and Harris, A. W. (1989). In *Asteroids II*, edited by R. P. Binzel, T. Gehrels, and M. S. Matthews (University of Arizona Press, Tucson), pp. 524–556.

Burns, J. A., Lamy, P. L., and Soter, S. (1979). Icarus **40**, 1.

Bus, S. J., Bowell, E., and French, L. M. (1988). IAU Circ. No. 4684.

Bus, S. J., Bowell, E., Harris, A. W., and Hewitt, A. V. (1989). Icarus **77**, 223.

Chapman, C. R., and Gaffey, M. J. (1979). In *Asteroids*, edited by T. Gehrels (University of Arizona Press, Tucson), pp. 655–687.

Cochran, A. L., Baker, E. S., and Cochran, W. D. (1980). Astron. J. **85**, 474.

Cowan, J. J., and A'Hearn, M. F. (1982). Icarus **50**, 53.

Dossin, F. (1966). Astron. J. **71**, 853.

Draine, B. T. (1985). Astrophys. J. Suppl. **57**, 587.

Edoh, O. (1983). Ph.D. thesis, University of Arizona.

Festou, M. C., Feldman, P. D., A'Hearn, M. F., Arpigny, C., Cosmovici, C. B., Danks, A.C., McFadden, L. A., Gilmozzi, R., Patriarchi, P., Tozzi, G. P., Wallis, M. K., and Weaver, H. A. (1986). Nature **321**, 361.

Gaffey, M. J., Bell, J. F., and Cruikshank, D. P. (1989). In *Asteroids II*, edited by R. P. Binzel, T. Gehrels, and M. S. Matthews (University of Arizona Press, Tucson), pp. 98–127.

Hardorp, J. (1978). Astron. Astrophys. **63**, 383.

Hardorp, J. (1980). Astron. Astrophys. **91**, 221.

Hartmann, W. K., Tholen, D. J., Meech, K., and Cruikshank, D. P. (1990). Icarus **83**, 1.

Huebner, W. F., and Giguere, P. T. (1980). Astrophys. J. **238**, 753.

Jewitt, D. C. (1990a). Astrophys. J. **351**, 277.

Jewitt, D. C. (1990b). In *Comets in the Post-Halley Era*, edited by R. Newburn, J. Rahe, and M. Neugebauer (Kluwer, Dordrecht) (in press).

Jewitt, D. C., and Luu, J. X. (1989). Astron. J. **97**, 1766.

Jewitt, D. C., and Luu, J. X. (1990). Astron. J. **100**, 933.

Khare, B. N., Sagan, C., Arakawa, E. T., Suits, F., Callcott, T. A., and Williams, M. W. (1984). Icarus **60**, 127.

Kowal, C. (1977). IAU Circ. No. 3129.

Krankowsky, D., Lämmerzahl, P., Herrwerth, I., Woweries, J., Eberhardt, P., Dolder, U., Herrman, U., Schulte, W., Berthelier, J. J., Illiano, J. M., Hodges, R. R., and Hoffman, J. H. (1986). Nature **321**, 326.

Kresák, L. (1979). In *Asteroids*, edited by T. Gehrels (University of Arizona Press, Tucson), pp. 289–309.

Lamy, P. L., and Perrin, J. M. (1988). Icarus **76**, 100.

Lamy, P. L., Grün E., and Perrin, J. M. (1987). Astron. Astrophys. **187**, 767.

Landolt, A. U. (1983). Astron. J. **88**, 439.

Lebofsky, L. A., Tholen, D. J., Rieke, G. H., and Lebofsky, M. J. (1984). Icarus **60**, 532.

Luu, J. X., and Jewitt, D. C. (1989). Bull. Am. Astron. Soc. **21**, 964.

Luu, J. X., and Jewitt, D. C. (1990). Astron. J. **99**, 1985.

Luu, J. X. (1990). Ph.D. thesis, Massachusetts Institute of Technology.

Massey, P., Strobel, K., Barnes, J. V., and Anderson, E. (1988). Astrophys. J. **328**, 315.

Meech, K., and Belton, M. (1989). IAU Circ. No. 4770.

Stone, R. P. S. (1977). Astrophys. J. **218**, 767.

Tholen, D. J., Hartmann, W. K., and Cruikshank, D. P. (1988). IAU Circ. No. 4554.

Tholen, D. J., and Barucci, M. A. (1989). In *Asteroids II*, edited by R. P. Binzel, T. Gehrels, and M. S. Matthews (University of Arizona Press, Tucson), pp. 298–315.

Thomas, N., and Keller, H. U. (1989). Astron. Astrophys. **213**, 487.

Thomas, P., and Veverka, J. (1980). Icarus **42**, 234.

van de Hulst, H. C. (1957). *Light Scattering by Small Particles* (Wiley, New York).

West, R. M. (1990). IAU Circ. No. 4970.

Wyckoff, S., and Wehinger, P. A. (1976). Astrophys. J. **204**, 604.

Wyckoff, S. (1982). In *Comets*, edited by L. Wilkening (University of Arizona Press, Tucson), pp. 3–55.

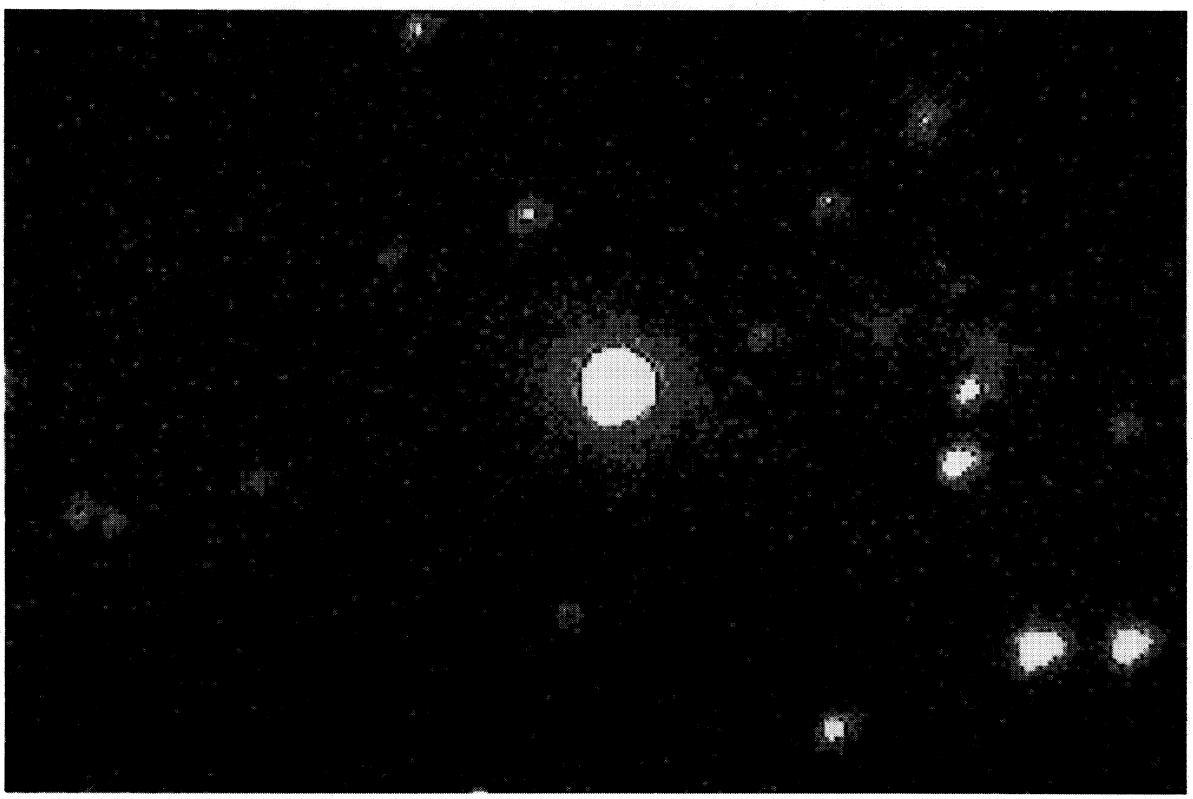

FIG. 2. A single 500 s integration of Chiron in the *R* filter, taken on UT 1990 January 29 with the UH 2.2 m telescope. North is to the right, west is to the bottom; the image is 38.0″ in the north–south direction and 25.4″ in the east–west direction, with an image scale of 0.2″/pixel. The coma is visible in the south–east and north–west directions.

J. X. Luu and D. C. Jewitt (see page 914)

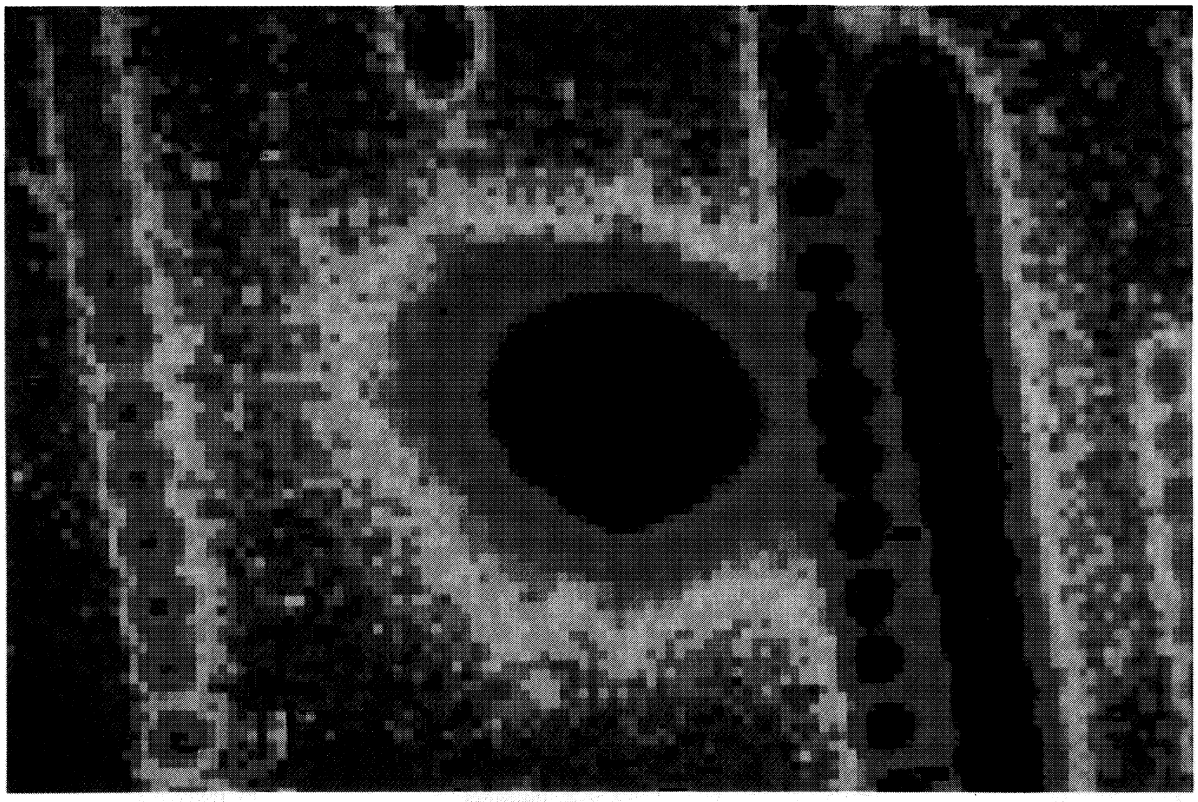

FIG. 9. A 20 000 s *R* integration of Chiron, formed by shifting and adding 40 separate CCD images of 500 s duration each. The data were taken UT 1990 January 29 at the UH 2.2 m telescope, with 0.2″ per pixel image scale and 0.8″ FWHM seeing. Stars and galaxies appear in rows due to the cancellation of the motion of Chiron with respect to the stars. An asymmetric coma is clearly apparent. The image has north to the right, west to the bottom, and is 25″ in width.

J. X. Luu and D. C. Jewitt (see page 919)